

Accelerated Article Preview

Inhibiting membrane rupture with NINJ1 antibodies limits tissue injury

Received: 21 November 2022

Accepted: 10 May 2023

Accelerated Article Preview

Cite this article as: Kayagaki, N. et al. Inhibiting membrane rupture with NINJ1 antibodies limits tissue injury. *Nature* <https://doi.org/10.1038/s41586-023-06191-5> (2023)

Nobuhiko Kayagaki, Irma B. Stowe, Kamela Alegre, Ishan Deshpande, Shuang Wu, Zhonghua Lin, Opher S. Kornfeld, Bettina L. Lee, Juan Zhang, John Liu, Eric Suto, Wyne P. Lee, Kellen Schneider, WeiYu Lin, Dhaya Seshasayee, Tushar Bhangale, Cecile Chalouni, Matthew C. Johnson, Prajakta Joshi, Jan Mossemann, Sarah Zhao, Danish Ali, Neil M. Goldenberg, Blayne A. Sayed, Benjamin E. Steinberg, Kim Newton, Joshua D. Webster, Ryan L. Kelly & Vishva M. Dixit

This is a PDF file of a peer-reviewed paper that has been accepted for publication. Although unedited, the content has been subjected to preliminary formatting. Nature is providing this early version of the typeset paper as a service to our authors and readers. The text and figures will undergo copyediting and a proof review before the paper is published in its final form. Please note that during the production process errors may be discovered which could affect the content, and all legal disclaimers apply.

1 **Inhibiting membrane rupture with NINJ1 antibodies limits tissue injury**

2

3 Nobuhiko Kayagaki^{1,12*}, Irma B. Stowe^{1,12}, Kamela Alegre¹, Ishan Deshpande^{1,2}, Shuang Wu³,
4 Zhonghua Lin³, Opher S. Kornfeld¹, Bettina L. Lee¹, Juan Zhang⁴, John Liu⁴, Eric Suto⁴, Wyne P.
5 Lee⁴, Kellen Schneider³, WeiYu Lin³, Dhaya Seshasayee³, Tushar Bhangale⁵, Cecile Chalouni⁶,
6 Matthew C. Johnson², Prajakta Joshi⁷, Jan Mossemann⁸, Sarah Zhao⁹, Danish Ali⁸, Neil M.
7 Goldenberg^{8,10}, Blayne A. Sayed^{8,11}, Benjamin E. Steinberg^{9,10}, Kim Newton¹, Joshua D. Webster⁶,
8 Ryan L. Kelly³, Vishva M. Dixit^{1*}

9

10 ¹Department of Physiological Chemistry, Genentech Inc., 1 DNA Way, South San Francisco,
11 California 94080, USA

12 ²Department of Structural Biology, Genentech Inc., 1 DNA Way, South San Francisco, California
13 94080, USA

14 ³Department of Antibody Engineering, Genentech Inc., 1 DNA Way, South San Francisco,
15 California 94080, USA

16 ⁴Department of Translational Immunology, Genentech Inc., 1 DNA Way, South San Francisco,
17 California 94080, USA

18 ⁵Department of Human Genetics, Genentech Inc., 1 DNA Way, South San Francisco, California
19 94080, USA

20 ⁶Department of Pathology, Genentech Inc., 1 DNA Way, South San Francisco, California 94080,
21 USA

22 ⁷Department of Biomolecular Resources, Genentech Inc., 1 DNA Way, South San Francisco,
23 California 94080, USA

24
25
26
27
28
29
30
31
32
33
34
35
36
37

⁸Program in Cell Biology, Hospital for Sick Children, 555 University Ave, Toronto, Ontario M5G 1X8, Canada

⁹Program in Neuroscience and Mental Health, Hospital for Sick Children, 555 University Ave, Toronto, Ontario M5G 1X8, Canada

¹⁰Department of Anesthesia and Pain Medicine, Hospital for Sick Children, 555 University Ave, Toronto, Ontario M5G 1X8, Canada

¹¹Division of General Surgery, Hospital for Sick Children, 555 University Ave, Toronto, Ontario M5G 1X8, Canada

¹²These authors contributed equally

* Correspondence to N.K. (kayagaki@gene.com) or V.M.D. (dixit@gene.com)

38 **Plasma membrane rupture (PMR) in dying cells undergoing pyroptosis or apoptosis requires**
39 **the cell-surface protein NINJ1¹. PMR releases proinflammatory cytoplasmic molecules,**
40 **collectively called damage-associated molecular patterns (DAMPs), that activate immune**
41 **cells. Therefore, inhibiting NINJ1 and PMR may limit the inflammation that is associated**
42 **with excessive cell death. Here we describe an anti-NINJ1 monoclonal antibody, specifically**
43 **targeting murine NINJ1, that blocks oligomerization of NINJ1 and prevents PMR. By**
44 **electron microscopy, this antibody prevented NINJ1 from forming oligomeric filaments. In**
45 **mice, inhibition of NINJ1 or *Ninj1* deficiency ameliorated hepatocellular PMR induced with**
46 **TNF plus D-Galactosamine, concanavalin A, Jo2 anti-Fas agonist antibody, or ischemia-**
47 **reperfusion injury (IRI). Accordingly, serum levels of lactate dehydrogenase (LDH), liver**
48 **enzymes alanine aminotransaminase (ALT) and aspartate aminotransferase (AST), and**
49 **DAMPs interleukin 18 (IL-18) and HMGB1 were reduced. Moreover, in the liver IRI model,**
50 **there was an attendant reduction in neutrophil infiltration. These data indicate that NINJ1**
51 **mediates PMR and inflammation in diseases driven by aberrant hepatocellular death.**

52
53 NINJ1 is a 16-kDa cell-surface protein predicted to have two transmembrane regions and N_{out}/C_{out}
54 topology^{2,3}. Although dispensable for cell death induction, NINJ1 controls an important
55 consequence of apoptotic or pyroptotic cell death, mediating PMR that non-selectively releases
56 proinflammatory cytoplasmic contents from dying cells^{1,4}. Whether NINJ1-dependent PMR
57 exacerbates tissue damage in disease is unclear, but *Ninj1* deficiency is reported to attenuate mouse
58 models of pulmonary fibrosis and multiple sclerosis^{5,6}. Given that a conserved extracellular region
59 of NINJ1 is essential for its oligomerization and PMR¹, we hypothesized that extracellular anti-
60 NINJ1 antibodies might be used to inhibit NINJ1-dependent PMR in vivo.

61

62 **Identifying NINJ1 blocking antibodies**

63 To generate NINJ1 blocking antibodies, *Ninj1*^{-/-} mice were immunized with extracellular vesicles
64 (EVs) expressing full-length mouse NINJ1 (Fig. 1a). We isolated approximately 15,000 NINJ1-
65 binding IgM⁻ B cells by flow cytometric analysis and characterized single cell supernatants for
66 binding to NINJ1-expressing cells. Functional screening of 217 recombinant anti-mouse NINJ1
67 IgG2a monoclonal antibodies identified clone D1 (*Ninj1*-575) as an inhibitor of NINJ1-dependent
68 PMR (Fig. 1b). Mouse bone marrow-derived macrophages (BMDMs) were primed with the Toll-
69 like receptor 2 (TLR2) agonist Pam3CSK4 to up-regulate inflammasome components, including
70 *Nlrp3*, and then cultured with 1 µg/mL anti-NINJ1 antibodies for 15 min prior to stimulation with
71 nigericin to activate NLRP3- and GSDMD-dependent pyroptosis^{7,8}. LDH release was used to
72 monitor NINJ1-dependent PMR¹. The most potent anti-NINJ1 antagonist antibody, clone D1,
73 reduced PMR in wild-type BMDMs to levels observed in *Ninj1*^{-/-} control BMDMs. The antigen-
74 binding fragment (Fab) of clone D1 also prevented nigericin-induced PMR in wild-type BMDMs,
75 suggesting that clone D1 can inhibit NINJ1 independently of binding to Fc receptors on the cell
76 surface (Extended Data Fig. 1a). Clone D1 or its Fab also suppressed membrane damage caused
77 by ectopic expression of mouse NINJ1, but not human NINJ1 in HEK293T cells (Fig. 1c and
78 Extended Data Fig. 1b).

79

80 We confirmed that clone D1 recognized mouse NINJ1, but not human NINJ1 by surface staining
81 and flow cytometric analysis of live HEK293T cells expressing N-terminally FLAG-tagged mouse
82 NINJ1 (Fig. 1d), or FLAG-tagged human NINJ1 (Extended Data Fig. 1c). Antibody binding to
83 mouse NINJ1 was abrogated by deletion of extracellular C-terminal residues 142-152 or by

84 substitution of residues 147-151 with alanines ($D_{147}VAPR \rightarrow A_{147}AAAA$). By contrast, deletion
85 of extracellular N-terminal residues 2-73 did not prevent the binding of clone D1. These data
86 indicate that clone D1 recognizes a C-terminal epitope in mouse NINJ1 (Extended Data Fig. 1d).
87 As a control, we used clone 25 anti-mouse NINJ1 antibody, which recognizes N-terminal residues
88 22-31¹. As expected, clone 25 immunolabeling of NINJ1-expressing cells was abrogated by
89 deletion of residues 2-73 of NINJ1 (Fig. 1d).

90
91 To extend our analyses in BMDMs, we monitored NINJ1-dependent PMR by time-lapse live-cell
92 imaging. Pam3CSK4-primed BMDMs were loaded with fluorescein isothiocyanate (FITC)-
93 conjugated 150 kDa dextran (DD-150) and dye release after nigericin stimulation was used as
94 indicator of PMR (Fig. 2a). Clone D1 reduced PMR in BMDMs in a dose-dependent manner
95 compared to an isotype control antibody. The clone D1 Fab also inhibited the release of DD-150
96 from nigericin-treated BMDMs (Extended Data Fig. 1e). Clone 25 exhibited PMR-blocking
97 activity¹, but was not as potent as clone D1 (Fig. 2a). Clones D1 and 25 also exhibited dose-
98 dependent inhibition of NINJ1-dependent PMR when measured by LDH release (Fig. 2b, lower
99 graphs). As expected, neither clone prevented nigericin-induced cell death based on the
100 measurement of cellular ATP levels (Fig. 2b, upper graphs). Morphologically, wild-type BMDMs
101 undergoing pyroptosis develop bubble-like herniations that burst in a NINJ1-dependent manner to
102 yield shrunken cellular corpses¹ (Fig. 2c). However, wild-type BMDMs treated with nigericin in
103 the presence of clone D1 or 25 resembled *Ninjl*^{-/-} BMDMs in that they exhibited a persistent
104 “bubble” morphology (Fig. 2c). Thus, NINJ1-blocking antibodies prevent PMR, but not formation
105 of membrane herniation during pyroptosis.

106

107 PMR is not limited to pyroptosis. BMDMs also undergo GSDMD-independent, but NINJ1-
108 dependent PMR after apoptotic blebbing and shrinkage, likely attributable to ATP depletion¹.
109 Accordingly, *Ninj1*^{-/-} BMDMs released less LDH than wild-type BMDMs following pyroptosis
110 induction with intracellular lipopolysaccharide (LPS) or flagellin, or after apoptosis induction with
111 doxorubicin, venetoclax, or tumor necrosis factor (TNF) plus actinomycin (Fig. 2d and Extended
112 Data Fig. 1f). Clone D1 also attenuated PMR, but not cell death, when wild-type BMDMs were
113 exposed to these pyroptotic or apoptotic stimuli. As expected¹, neither *Ninj1* deficiency nor clone
114 D1 reduced LDH release following necroptosis induction with TNF plus the pan-caspase inhibitor
115 zVAD (Extended Data Fig. 1f). These results establish anti-mouse NINJ1 antibody clone D1 as a
116 potent inhibitor of PMR associated with apoptosis or pyroptosis. A commercial anti-NINJ1
117 antibody (BD Bioscience clone 50) and a NINJ1₂₆₋₃₇ peptide have been used to block mouse NINJ1
118 in vivo⁹⁻¹¹, but neither blocked nigericin-induced PMR in BMDMs (Extended Data Fig. 2a, b, c).
119 Furthermore, BD clone 50 failed to bind to mouse NINJ1 expressed in HEK293T cells (Extended
120 Data Fig. 2d). Therefore, clone D1 appears to be unique in its ability to potently block NINJ1-
121 dependent PMR (Fig. 1b).

122

123 **Clone D1 blocks NINJ1 oligomerization**

124 We hypothesized that clone D1 blocked PMR in BMDMs by preventing oligomerization of
125 NINJ1¹. In keeping with such a mechanism, nigericin induced speck-like assemblies of NINJ1 in
126 wild-type BMDMs, but these were less prevalent in the presence of a clone D1 Fab (Fig. 3a, b).

127 We also looked at the effect of clone D1 on N-terminally FLAG-tagged mouse NINJ1 purified
128 from transiently transfected human Expi293F cells. By size exclusion chromatography (SEC),
129 purified FLAG-NINJ1 migrated as a high molecular weight species (peak at 8.5 ml retention

130 volume) (Fig. 3c, Extended Data Fig. 3a, b). Negative stain electron microscopy (ns-EM) of the
131 FLAG-NINJ1 revealed that NINJ1 formed oligomeric structures with heterogeneous shapes,
132 including rings, filaments, clusters, and arcs up to 200 nm in size (Fig. 3d). In contrast, when
133 FLAG-NINJ1 was co-expressed with clone D1 Fab, the purified NINJ1-Fab complex migrated as
134 a lower molecular weight species (peak at 15 ml retention volume) (Fig. 3c, Extended Data Fig.
135 3a, b) and showed no high-order oligomeric structure formation in ns-EM (Fig. 3d). Thus, binding
136 of clone D1 Fab to NINJ1 prevents it from assembling into larger oligomeric structures.

137
138 Purified FLAG-NINJ1 added to synthetic liposome membranes caused the release of an
139 encapsulated cargo, whereas the NINJ1-D1 Fab complex did not (Fig. 3e). These data suggest that
140 NINJ1 forms lytic higher order oligomers, which can be prevented by clone D1. The formation of
141 higher order oligomeric filaments is not without precedent and has been reported for multiple
142 apoptotic, pyroptotic, and necroptotic molecules, including ASC and caspase-8^{12,13}. We propose
143 that oligomeric assemblies of NINJ1 mediate PMR in cells and clone D1 binding to NINJ1
144 prevents these oligomers from forming. Clone 25 resembled clone D1 in preventing NINJ1-
145 dependent cargo release from liposomes (Fig. 3e) and NINJ1 filaments by ns-EM (Extended Data
146 Fig. 3c), but was not as efficient as clone D1 at preventing the oligomeric assembly of NINJ1 in
147 SEC analysis (Extended Data Fig. 3d). These data are consistent with clone 25 being a weaker
148 antagonist than clone D1 in cellular PMR assays (Fig. 2a, b). Neither the C-terminal residues of
149 NINJ1 recognized by clone D1, nor the N-terminal residues bound by clone 25, are resolved in the
150 cryo-EM structure of NINJ1 filaments reported by Degen et al (manuscript accepted at Nature),
151 suggesting that these regions of NINJ1 are flexible and potentially dispensable for oligomerization.
152 Indeed, alanine mutations within these regions did not suppress membrane damage caused by

153 ectopic expression of NINJ1¹. Therefore, binding of clone D1 or clone 25 to NINJ1 may prevent
154 NINJ1 oligomerization through steric hindrance.

155

156 **Targeting PMR in mouse hepatitis models**

157 The role of NINJ1-dependent PMR in human disease and inflammation is unclear, but genome-
158 wide association studies¹⁴ suggest a link between *NINJ1* and lower serum levels of the liver
159 enzymes ALT and AST, two clinically important biomarkers of hepatocellular injury or membrane
160 damage^{15,16} (Extended Data Fig. 4). TNF-induced hepatocyte apoptosis causes liver inflammation,
161 and has been implicated in multiple diseases including hepatocellular carcinoma, ischemia, and
162 viral hepatitis¹⁷. To address the role of NINJ1 in apoptosis-associated PMR in vivo, we assessed
163 *Ninj1*^{fl/fl} *Rosa26-CreER*^{T2} mice in a model of fulminant hepatitis. This mouse strain allows
164 tamoxifen-induced, systemic *Ninj1* deletion in adults (Extended Data Fig. 5a, b), and therefore
165 avoids the developmental hydrocephalus that is observed in a significant fraction of *Ninj1*^{-/-}
166 newborns⁵. After tamoxifen treatment, *Ninj1*^{fl/fl} *Rosa26-CreER*^{T2} mice and *Rosa26-CreER*^{T2}
167 control animals were dosed with TNF and the transcriptional inhibitor D-Galactosamine (D-Gal)
168 to induce hepatocyte apoptosis¹⁸⁻²⁰. TNF plus D-Gal caused fulminant hepatocellular PMR in
169 *Rosa26-CreER*^{T2} mice as measured by increased serum ALT, AST, and LDH (Fig. 4a). The sera
170 of *Ninj1*-deficient mice treated with TNF plus D-Gal contained significantly less ALT, AST, and
171 LDH. Histological analysis of control livers revealed that TNF plus D-Gal caused massive lesions
172 characterized by pyknotic hepatocellular death with hemorrhage (Fig. 4b, c). Immunolabeling
173 showed that these lesions were positive for cleaved caspase-3, a marker of apoptosis (Fig. 4d).
174 *Ninj1* deficiency did not abate TNF plus D-Gal-induced hepatocellular degeneration and caspase-
175 3 cleavage (Fig. 4b, c, d), consistent with the post-apoptotic role of NINJ1¹. Although mortality

176 was not delayed in this acute liver injury model (Extended Data Fig. 6a), a greater proportion of
177 *Ninj1*-deficient hepatocytes exhibited the swollen morphology associated with PMR malfunction
178 (Fig. 4b, c). These data indicate that NINJ1 mediates apoptosis-related PMR in vivo.

179
180 Next, we determined whether clone D1 could limit liver injury induced by TNF plus D-Gal. Wild-
181 type mice dosed with an isotype control antibody 2 h prior to injection of TNF plus D-Gal exhibited
182 markedly elevated ALT, AST, and LDH serum levels, indicative of robust hepatocellular PMR
183 (Fig. 4e). Similar to *Ninj1* deficiency, pretreatment with clone D1 significantly attenuated TNF
184 plus D-Gal-induced increases in serum LDH, ALT, and AST (Fig. 4e). Clone D1 also caused TNF
185 and D-Gal-treated hepatocytes to have a ballooned morphology, whereas degeneration of the liver
186 and the extent of caspase-3 cleavage was comparable to that in livers pre-treated with the isotype
187 control antibody (Extended Data Fig. 6b, c, d). The presence of similar numbers of cleaved
188 caspase-3-positive cells in control and D1 treated (or *Ninj1*-deficient) mice suggests that NINJ1
189 inhibition does not alter the clearance of dead cells by phagocytes. Indeed, adult *Ninj1*-deficient
190 mice do not develop the spontaneous inflammation that is typical of mice with defective
191 efferocytosis²¹.

192
193 TNF-dependent activation of apoptosis in D-Gal-sensitized hepatocytes relies on caspase-8²²,
194 which also cleaves and activates leaderless IL-18²³⁻²⁵, but the mechanism by which IL-18, and
195 potentially other DAMPs, are released from apoptotic cells is ill-defined. We found that TNF plus
196 D-Gal increased IL-18 and HMGB1 DAMP²⁶ levels in the serum in a NINJ1-dependent manner
197 (Fig. 4f, g). *Ninj1* deficiency or pretreatment of mice with clone D1 both held serum IL-18 and
198 HMGB1 in check after TNF plus D-Gal dosing. These data strongly suggest that PMR mediated

199 by NINJ1 releases IL-18 into the serum in this apoptosis-driven liver injury model. This
200 mechanism differs from that in pyroptotic BMDMs, wherein GSDMD pores²⁷ suffice to release
201 IL-18 and other small DAMPs independently of NINJ1¹. Although the role of GSDMD pores in
202 IL-18 release in vivo still remains uncertain, our data indicate that both NINJ1-dependent and -
203 independent mechanisms may release small DAMPs in disease.

204

205 We also investigated the effect of clone D1 in mouse hepatitis instigated by either the T cell
206 mitogen concanavalin A (ConA)²⁸, Jo2 anti-Fas agonistic antibody²⁹, or ischemia-reperfusion
207 injury (IRI)³⁰. *Ninjl*-deficient mice or mice pre-treated with clone D1 exhibited less serum LDH,
208 ALT, AST, IL-18, or HMGB1 than control mice at 8 or 18 hours after ConA dosing (Fig. 4 h, i,
209 Extended Data Fig. 7a, b), after hepatic IRI (Extended Data Fig. 7c, d), and after Jo2 injection
210 (Extended Data Fig. 7e). As expected, clone D1 did not prevent hepatocellular degeneration and
211 the appearance of cleaved caspase-3-positive cells after ConA dosing (Extended Data Fig. 7f, g),
212 nor confluent necrosis after IRI injury (Extended Data Fig. 7h). Importantly, we observed NINJ1-
213 dependent neutrophil recruitment into the damaged liver after IRI (Extended Data Fig. 7i), in
214 agreement with a recent study³¹ using *Ninjl*-deficient mice that was published during the revision
215 of our manuscript. Collectively, these data suggest that NINJ1 mediates hepatocellular PMR and
216 promotes inflammation in vivo.

217

218 Identification of antagonist anti-NINJ1 monoclonal antibodies that can prevent the assembly of
219 lytic NINJ1 oligomers, and thereby limit PMR and the release of proinflammatory DAMPs in vivo,
220 indicates that it is possible to target a post-cell death event. Although clone D1 treatment attenuated
221 PMR in vivo, its efficacy was evaluated in acute mouse hepatitis models. The impact of NINJ1

222 blockade in settings of chronic inflammation, where protracted DAMP release is expected to
223 exacerbate pathology, will be an exciting area of future investigation, but will require reagents
224 with improved pharmacokinetic properties. We were unable to sustain serum levels of clone D1
225 long-term by repeat dosing.

226

227

ACCELERATED ARTICLE PREVIEW

228 **Figure Legends**

229

230 **Figure 1 | Identification of NINJ1 blocking antibody clone D1**

231 **a**, Scheme of recombinant antibody screening. EV, extracellular vesicle. NGS, next-generation
232 sequencing.

233 **b**, Graph shows LDH released from Pam3CSK4-primed wild-type BMDMs after nigericin
234 stimulation for 16 h in the presence of 1 $\mu\text{g}/\text{mL}$ antibody. The white circle non-stimulated wild-
235 type BMDMs, the black circle primed and stimulated *Ninj1*^{-/-} BMDMs, the dark grey circle clone
236 25, the blue circle clone D1, and the light grey circles other anti-NINJ1 antibodies. The LDH score
237 is the LDH release normalized against the no antibody control.

238 **c**, Graphs indicate the percentage of YOYO-1⁺ HEK293T cells expressing NINJ1 when cultured
239 with clone D1 or an isotype control antibody. Circles are the mean \pm s.d. (shaded area) of 3
240 independent replicates.

241 **d**, Flow cytometry histograms of propidium iodide-negative HEK293T cells surface-stained with
242 anti-NINJ1 or anti-FLAG antibodies. Cells are mock transfected (light gray) or transfected with
243 the NINJ1 constructs indicated (dark gray). Results are representative of 3 independent
244 experiments (**c**, **d**).

245

246 **Figure 2 | Clone D1 potently inhibits NINJ1-dependent PMR**

247 **A**, Graphs show the release of DD-150 from Pam3CSK4-primed BMDMs after nigericin
248 stimulation. Data are means (circles) \pm s.d. (shaded area) of biological replicates ($n = 3$ animals);
249 data were generated with bone marrow harvested from 3 different mice.

250 **b, d**, Graphs indicate cell viability (top) or LDH release (bottom) in BMDM cultures following
251 pyroptosis induction with nigericin (**b**) or cytoplasmic LPS for 3 h, apoptosis induction with
252 doxorubicin for 6 h, or TNF + actinomycin D for 6 h. Act, actinomycin D (**d**). Pyroptotic stimuli
253 were applied to Pam3CSK4-primed BMDMs. Bars are the mean of 3 biological replicates ($n = 3$
254 animals) (**b, d**) as in **a**.

255 **c**, Bright-field images of Pam3CSK4-primed BMDMs stimulated with nigericin for 8 h. Scale bar,
256 25 μm . Results representative of 3 independent experiments (**a, b, c, d**).

257

258 **Figure 3 | Clone D1 attenuates NINJ1 oligomerization**

259 **a**, Immunolabelling of endogenous NINJ1 in BMDMs after priming with Pam3CSK4 and then
260 stimulation with nigericin for 45 min in the presence or absence (cont) of clone D1 Fab.
261 Arrowheads highlight representative NINJ1 specks.

262 **b**, Quantification of the percentage of cells bearing NINJ1 specks in (**a**). Bars indicate the mean.
263 D1 Fab, $n = 10$ independent samples; the others, $n = 20$ independent samples. P value two-tailed
264 t -test, $P = 0.0000091$.

265 **c**, Size exclusion chromatography traces for purified NINJ1 or the NINJ1-clone D1 Fab complex.
266 Molecular weight standard marker positions are pointed by arrows. Results representative of 3
267 independent experiments.

268 **d**, Negative stain electron microscopy of NINJ1 or the NINJ1-clone D1 Fab complex in (**c**).

269 **e**, Liposome cargo release by the NINJ1 or NINJ1-D1 Fab complex in (**c**) or NINJ1-clone 25 Fab
270 complex in Extended Data Fig. 3d. Bars are the mean of 3 independent replicates (circles). P value
271 two-tailed Mann–Whitney U -test, $P = 0.0000411$ (NINJ1 + clone 25 Fab v NINJ1 alone), $P =$

272 0.0000411 (NINJ1 + clone D1 Fab v NINJ1 alone). 100% cargo release is defined by total cargo
273 release mediated by 1% CHAPSO.

274

275 **Figure 4 | Clone D1 limits NINJ1-dependent PMR and DAMP release in vivo**

276 **a**, Mouse serum LDH, ALT, and AST. Where indicated, mice were dosed for 7 h with TNF and
277 D-Gal. a.u., arbitrary units. Untreated wild-type, $n = 5$ mice; tamoxifen-treated groups, $n = 6$ mice.
278 P value two-tailed unpaired t -test, $P = 0.0000000000665$ (LDH), $P = 0.00000296$ (ALT), $P =$
279 0.000000000067 (AST).

280 **b**, Representative haematoxylin and eosin-stained liver sections of the mice in **(a)**. Scale bar, 25
281 μm .

282 **c**, Histological scoring of mouse livers. Untreated wild-type, $n = 3$ mice; tamoxifen-treated groups,
283 $n = 7$ (left) or 6 (right) mice. P value two-tailed Mann–Whitney U -test.

284 **d**, Mouse liver sections with immunolabeling of cleaved caspase-3 (brown). Graph indicates
285 qualitative scoring of cleaved caspase-3 labeling. Untreated wild-type, $n = 2$ mice; tamoxifen-
286 treated groups, $n = 7$ mice. P value two-tailed Mann–Whitney U -test. Scale bar, 100 μm .

287 **e, h**, Wild-type mouse serum LDH, ALT, and AST. Where indicated, mice were dosed with 50
288 mg kg^{-1} antibody for 2 h before dosing with TNF plus D-Gal for 6 h **(e)** or ConA for 8 h **(h)**.
289 Untreated wild-type, $n = 5$ **(e)** or $n = 4$ mice **(h)**; wild-type dosed with antibodies, $n = 10$ mice. P
290 value two-tailed unpaired t -test. **e**, $P = 0.00000915$ (LDH), $P = 0.000094$ (ALT).

291 **f, g, i**, Mouse serum IL-18 and HMGB1 of the mice in **(a)**, **(e)**, and **(h)**, respectively. Untreated
292 wild-type, $n = 5$ mice; tamoxifen-treated $Ninj1^{+/+}$ $Rosa26\text{-CreER}^{\text{T2}}$, $n = 5$ (left), $n = 6$ (right) mice;
293 tamoxifen-treated $Ninj1^{\text{fl/fl}}$ $Rosa26\text{-CreER}^{\text{T2}}$, $n = 6$ **(f)**. Untreated wild-type, $n = 5$ **(g)** or $n = 4$ **(i)**

294 mice; treated groups, $n = 10$ mice (**g, i**). P value two-tailed Mann-Whitney U -test (**f**), two-tailed
295 unpaired t -test (**g, i**). **g**, $P = 0.00000682$.

296 Lines indicate the mean, circles individual mice (**a, c, d, e, h, f, g, i**).

297

298

299

ACCELERATED ARTICLE PREVIEW

300 **References**

- 301 1 Kayagaki, N. *et al.* NINJ1 mediates plasma membrane rupture during lytic cell death.
302 *Nature* **591**, 131-136, doi:10.1038/s41586-021-03218-7 (2021).
- 303 2 Araki, T. & Milbrandt, J. Ninjurin, a novel adhesion molecule, is induced by nerve injury
304 and promotes axonal growth. *Neuron* **17**, 353-361, doi:10.1016/s0896-6273(00)80166-x
305 (1996).
- 306 3 Araki, T., Zimonjic, D. B., Popescu, N. C. & Milbrandt, J. Mechanism of homophilic
307 binding mediated by ninjurin, a novel widely expressed adhesion molecule. *J Biol Chem*
308 **272**, 21373-21380, doi:10.1074/jbc.272.34.21373 (1997).
- 309 4 Bjanes, E. *et al.* Genetic targeting of Card19 is linked to disrupted NINJ1 expression,
310 impaired cell lysis, and increased susceptibility to Yersinia infection. *PLoS Pathog* **17**,
311 e1009967, doi:10.1371/journal.ppat.1009967 (2021).
- 312 5 Ahn, B. J. *et al.* Ninjurin1 deficiency attenuates susceptibility of experimental autoimmune
313 encephalomyelitis in mice. *J Biol Chem* **289**, 3328-3338, doi:10.1074/jbc.M113.498212
314 (2014).
- 315 6 Choi, S. *et al.* Ninjurin1 Plays a Crucial Role in Pulmonary Fibrosis by Promoting
316 Interaction between Macrophages and Alveolar Epithelial Cells. *Sci Rep* **8**, 17542,
317 doi:10.1038/s41598-018-35997-x (2018).
- 318 7 Mariathasan, S. *et al.* Cryopyrin activates the inflammasome in response to toxins and
319 ATP. *Nature* **440**, 228-232, doi:10.1038/nature04515 (2006).
- 320 8 Kayagaki, N. *et al.* Caspase-11 cleaves gasdermin D for non-canonical inflammasome
321 signalling. *Nature* **526**, 666-671, doi:10.1038/nature15541 (2015).
- 322 9 Zhang, H. *et al.* Role of NINJ1 in Gout Flare and Potential as a Drug Target. *J Inflamm*
323 *Res* **15**, 5611-5620, doi:10.2147/JIR.S378341 (2022).
- 324 10 Yin, G. N. *et al.* Inhibition of Ninjurin 1 restores erectile function through dual angiogenic
325 and neurotrophic effects in the diabetic mouse. *Proc Natl Acad Sci U S A* **111**, E2731-2740,
326 doi:10.1073/pnas.1403471111 (2014).
- 327 11 Jung, H. J. *et al.* Detrimental Role of Nerve Injury-Induced Protein 1 in Myeloid Cells
328 under Intestinal Inflammatory Conditions. *Int J Mol Sci* **21**, doi:10.3390/ijms21020614
329 (2020).

- 330 12 Lu, A. *et al.* Unified polymerization mechanism for the assembly of ASC-dependent
331 inflammasomes. *Cell* **156**, 1193-1206, doi:10.1016/j.cell.2014.02.008 (2014).
- 332 13 Fu, T. M. *et al.* Cryo-EM Structure of Caspase-8 Tandem DED Filament Reveals Assembly
333 and Regulation Mechanisms of the Death-Inducing Signaling Complex. *Molecular cell* **64**,
334 236-250, doi:10.1016/j.molcel.2016.09.009 (2016).
- 335 14 Sinnott-Armstrong, N. *et al.* Genetics of 35 blood and urine biomarkers in the UK Biobank.
336 *Nat Genet* **53**, 185-194, doi:10.1038/s41588-020-00757-z (2021).
- 337 15 Ozer, J., Ratner, M., Shaw, M., Bailey, W. & Schomaker, S. The current state of serum
338 biomarkers of hepatotoxicity. *Toxicology* **245**, 194-205, doi:10.1016/j.tox.2007.11.021
339 (2008).
- 340 16 McGill, M. R. The past and present of serum aminotransferases and the future of liver
341 injury biomarkers. *EXCLI J* **15**, 817-828, doi:10.17179/excli2016-800 (2016).
- 342 17 Tiegs, G. & Horst, A. K. TNF in the liver: targeting a central player in inflammation. *Semin*
343 *Immunopathol* **44**, 445-459, doi:10.1007/s00281-022-00910-2 (2022).
- 344 18 Lehmann, V., Freudenberg, M. A. & Galanos, C. Lethal toxicity of lipopolysaccharide and
345 tumor necrosis factor in normal and D-Galactosamine-treated mice. *J Exp Med* **165**, 657-
346 663, doi:10.1084/jem.165.3.657 (1987).
- 347 19 Leist, M. *et al.* Murine hepatocyte apoptosis induced in vitro and in vivo by TNF-alpha
348 requires transcriptional arrest. *J Immunol* **153**, 1778-1788 (1994).
- 349 20 Keppler, D. O., Pausch, J. & Decker, K. Selective uridine triphosphate deficiency induced
350 by D-Galactosamine in liver and reversed by pyrimidine nucleotide precursors. Effect on
351 ribonucleic acid synthesis. *J Biol Chem* **249**, 211-216 (1974).
- 352 21 Peng, Y. & Elkon, K. B. Autoimmunity in MFG-E8-deficient mice is associated with
353 altered trafficking and enhanced cross-presentation of apoptotic cell antigens. *J Clin Invest*
354 **121**, 2221-2241, doi:10.1172/JCI43254 (2011).
- 355 22 Kaufmann, T. *et al.* Fatal hepatitis mediated by tumor necrosis factor TNFalpha requires
356 caspase-8 and involves the BH3-only proteins Bid and Bim. *Immunity* **30**, 56-66,
357 doi:10.1016/j.immuni.2008.10.017 (2009).
- 358 23 Bossaller, L. *et al.* Cutting edge: FAS (CD95) mediates noncanonical IL-1beta and IL-18
359 maturation via caspase-8 in an RIP3-independent manner. *J Immunol* **189**, 5508-5512,
360 doi:10.4049/jimmunol.1202121 (2012).

- 361 24 Uchiyama, R., Yonehara, S. & Tsutsui, H. Fas-mediated inflammatory response in *Listeria*
362 monocytogenes infection. *J Immunol* **190**, 4245-4254, doi:10.4049/jimmunol.1203059
363 (2013).
- 364 25 Nakanishi, K., Yoshimoto, T., Tsutsui, H. & Okamura, H. Interleukin-18 regulates both
365 Th1 and Th2 responses. *Annu Rev Immunol* **19**, 423-474,
366 doi:10.1146/annurev.immunol.19.1.423 (2001).
- 367 26 Andersson, U. & Tracey, K. J. HMGB1 is a therapeutic target for sterile inflammation and
368 infection. *Annu Rev Immunol* **29**, 139-162, doi:10.1146/annurev-immunol-030409-101323
369 (2011).
- 370 27 Xia, S. *et al.* Gasdermin D pore structure reveals preferential release of mature interleukin-
371 1. *Nature*, doi:10.1038/s41586-021-03478-3 (2021).
- 372 28 Ksontini, R. *et al.* Disparate roles for TNF-alpha and Fas ligand in concanavalin A-induced
373 hepatitis. *J Immunol* **160**, 4082-4089 (1998).
- 374 29 Ogasawara, J. *et al.* Lethal effect of the anti-Fas antibody in mice. *Nature* **364**, 806-809,
375 doi:10.1038/364806a0 (1993).
- 376 30 Hirao, H., Nakamura, K. & Kupiec-Weglinski, J. W. Liver ischaemia-reperfusion injury: a
377 new understanding of the role of innate immunity. *Nat Rev Gastroenterol Hepatol* **19**, 239-
378 256, doi:10.1038/s41575-021-00549-8 (2022).
- 379 31 Hu, Y. *et al.* The *Ninj1/Dusp1* Axis Contributes to Liver Ischemia Reperfusion Injury by
380 Regulating Macrophage Activation and Neutrophil Infiltration. *Cell Mol Gastroenterol*
381 *Hepatol* **15**, 1071-1084, doi:10.1016/j.jcmgh.2023.01.008 (2023).
- 382 32 Bycroft, C. *et al.* The UK Biobank resource with deep phenotyping and genomic data.
383 *Nature* **562**, 203-209, doi:10.1038/s41586-018-0579-z (2018).
384

385 **Methods**

386 **Mice**

387 All animal procedures were conducted under protocols approved by the Genentech Institutional
388 Animal Care and Use Committee in an Association for Assessment and Accreditation of
389 Laboratory Animal Care (AAALAC)-accredited facility in accordance with the Guide for the Care
390 and Use of Laboratory Animals and applicable laws and regulations. All animal procedures related
391 to hepatic ischemia-reperfusion injury were conducted under protocols approved by the Animal
392 Care Committee at The Hospital for Sick Children and in accordance with animal care regulation
393 and policies of the Canadian Council on Animal Care. *Ninj1*^{-/-} mice with a C57BL/6N background
394 were described previously¹. Wild-type mice (that have two alleles of wild-type *Ninj1*, *Ninj1*^{+/+})
395 were littermates. *Ninj1*^{fl/fl} with exon 3 floxed were generated by Ozgene (Australia) from C57BL/6
396 ES cells. *Ninj1*^{fl/+} mice were genotyped with PCR primers (5'-TAG TTA GTT CAA GCC AGA
397 G and 5'-GCG GTCA GCA GAA TAG A, and 5'-CCA AGG AAG CAG GTA C) yielding 396
398 bp wild-type, 448 bp floxed, and 359 bp knockout DNA fragments. *Ninj1*^{fl/fl} mice were bred with
399 *Rosa26*^{Cre.ERT2/+} C57BL/6 mice³³.

400

401 For in vivo studies (described below), *Ninj1*^{fl/fl} mice rather than *Ninj1*^{-/-} mice were used to avoid
402 the developmental hydrocephalus that is observed in a significant fraction of *Ninj1*^{-/-} newborns⁵.
403 *Ninj1*^{fl/fl} *Rosa26*^{Cre.ERT2/+} and *Ninj1*^{+/+} *Rosa26*^{Cre.ERT2/+} siblings aged 6-9 weeks were dosed daily by
404 intraperitoneal (ip) injection with 80 mg kg⁻¹ body weight of tamoxifen in sunflower oil
405 (MilliporeSigma) for 5 consecutive days. Experiments and analyses were performed two weeks
406 after the final dose of tamoxifen.

407 Mice were housed in individually ventilated cages within animal rooms maintained on a 14:10-
408 hour, light:dark cycle with ad libitum access to food and water. Animal rooms were temperature
409 and humidity-controlled, between 68-79°F and 30-70% respectively, with 10 to 15 room air
410 exchanges per hour.

411

412 **Generation of EVs and recombinant mouse NINJ1**

413 Expi293F cells (Thermo Fisher Scientific) were co-transfected with pRK-FLAG-mNINJ1
414 (Genentech) and a mammalian expression vector encoding HIV-1/MLV Gag³⁴. EVs were purified
415 from the supernatant 7 days post-transfection using ultracentrifugation³⁵.

416

417 For recombinant NINJ1 production, Expi293F suspension cells were cultured in Expi293
418 Expression Medium (Thermo Fisher Scientific) and transfected with pRK-FLAG-mNINJ1 using
419 the ExpiFectamine 293 transfection kit (Thermo Fisher Scientific). Frozen cell pellets (50 g) were
420 thawed and washed with a hypotonic buffer containing 20 mM HEPES pH 7.5, 1 mM EDTA,
421 supplemented with leupeptin, benzamidine and protease inhibitor tablets (Roche). Cells were
422 solubilized with 50 mM HEPES pH 7.5, 300 mM NaCl, 1% (w/v) lauryl maltose neopentyl glycol
423 (LMNG, Anatrace), 0.1% (w/v) cholesteryl hemisuccinate (CHS, Anatrace), supplemented with
424 leupeptin, benzamidine and Roche protease inhibitor tablets for 1.5 h at 4°C under gentle agitation.
425 After ultracentrifugation at 185,000 x g for 1 h, the supernatant was gently rotated with anti-FLAG
426 M2 affinity resin (Sigma) for 1 h at 4°C. Unbound proteins were washed away with 10 column
427 volumes (CV) of wash buffer A (50 mM HEPES pH 7.5, 300 mM NaCl, 0.1% (w/v) LMNG,
428 0.01% (w/v) CHS), followed by 10 CV of wash buffer B (50 mM HEPES pH 7.5, 150 mM NaCl,
429 0.005% (w/v) LMNG, 0.0005% (w/v) CHS). Recombinant NINJ1 was eluted with 5 CV of wash

430 buffer B supplemented with 300 µg/mL FLAG peptide (MilliporeSigma). Eluate was concentrated
431 in a 50 kDa MWCO concentrator and loaded onto a Superose6 Increase 10/300 GL column (GE
432 Healthcare) equilibrated with 20 mM HEPES pH 7.5, 150 mM NaCl, 0.005% (w/v) LMNG,
433 0.0005% (w/v) CHS. Recombinant NINJ1 was conjugated to Alexa Fluor 647 with a Lightning-
434 Link® Alexa Fluor 647 kit (Novus Biologicals).

435

436 **Anti-mouse NINJ1 antibody generation and screening**

437 *Ninj1*^{-/-} mice were immunized biweekly with mouse NINJ1-expressing EVs (extracellular
438 vesicles) plus Ribi adjuvant (MilliporeSigma) and mouse plasmids encoding mouse NINJ1 (in
439 pCAGGS vector, Genentech), Flt3L (in pORF vector, Genentech) and mouse GM-CSF (in pORF
440 vector, Genentech). Sera from immunized mice were tested by flow cytometry for reactivity
441 towards mouse NINJ1-expressing BALB/3T3 cells (clone A31, ATCC CCL-163). B cells from
442 the lymph nodes and spleens of immunized mice were enriched using a cocktail of depletion
443 antibodies (biotinylated CD11b at 1:400, CD11c at 1:400, Ly-6G/C at 1:400, CD49b at 1:400,
444 Ter119 at 1:100, CD4 at 1:200, CD8b.2 at 1:200, CD11b at 1:400 from BD Biosciences) and
445 magnetic streptavidin beads (Miltenyi Biotec). Enriched cells were stained with PE-Cy7-
446 conjugated rat anti-mouse IgM (BD Pharmingen, 1:50-100), rat anti-mouse B220 eFluor 450
447 (Thermo Fisher Scientific, 1:50), and AF647-labeled mouse NINJ1. Approximately 15,000
448 NINJ1-bound IgM⁻B220⁺ B cells were single cell-sorted into 96-well plates containing
449 supplemented RPMI 1640 medium (Thermo Fisher Scientific) and EL-4-B5 feeder cells (Roche).
450 After 8 to 10 days in culture, supernatants were screened for mouse NINJ1-reactive IgGs using an
451 IgG ELISA (Rockland) and flow cytometry against NINJ1-expressing 3T3 cells. B cells producing
452 NINJ1-reactive IgGs were the starting point for the generation of 217 recombinant monoclonal

453 antibodies using published methods³⁶. Briefly, RNA was extracted from the B cells using a
454 MagMaxTM-96 Total RNA Isolation Kit (Thermo Fisher Scientific). Variable light (VL) and
455 variable heavy (VH) domains were PCR-amplified from cDNA using a forward barcoded primer
456 set recognizing the leader sequence of most known mouse variable genes, and a barcoded reverse
457 primer recognizing the constant domain³⁷. Individual purified VL and VH PCR products were
458 pooled for next-generation sequencing library preparation using the Ovation[®] Library System for
459 Low Complexity Samples kit (Nugen). A MiSeq sequencer (Illumina) was used for 2x300 bp
460 paired sequencing. VH and VL sequences were synthesized (Genscript) and cloned into pRK
461 mammalian expression vectors encoding the mouse γ 2a and k constant domains, respectively³⁷.
462 Recombinant antibodies were transiently expressed in CHO cells and purified on a protein A
463 column³⁸. Briefly, CHO cells (Genentech) were seeded at $0.4-0.8 \times 10^6$ cells/ml. After three or
464 four days later, cells were transfected with plasmids by using PEIPro (Polyplus) according to
465 manufacture's instruction. Culture supernatants were harvested 14 days post transfection.
466 Recombinant antibodies were screened for NINJ1 inhibitory activity by LDH release assay in
467 BMDMs. Antibodies (1 μ g/mL) were added to Pam3CSK4-primed BMDMs for 15 min prior to
468 nigericin stimulation. At 16 h post stimulation, supernatants were collected for LDH release assays.

469

470 **Reagents**

471 Ultra-pure LPS (*E. coli* O111:B4, InvivoGen), Pam3CSK4 (InvivoGen), nigericin (InvivoGen),
472 ultra-pure flagellin (from *P. aeruginosa*, InvivoGen), venetoclax (TOCRIS), doxorubicin (Enzo
473 Life Sciences), mouse TNF (Genentech), actinomycin D (Act, EMD Millipore), Z-VAD-FMK
474 (zVAD; Promega). Antibodies used for western blotting were rabbit anti-mouse NINJ1 clone 25
475 (Ninj1-25, Genentech, 0.2 μ g/mL)¹, β -actin HRP (AC-15, Novus Biologicals, 0.1 μ g/mL), HRP-

476 anti-rabbit F(ab')₂ fragment (Jackson Immunoresearch, 1:5000), and HRP-anti rabbit Fc fragment
477 (Jackson Immunoresearch, 1:5000). A list of all antibodies used in this manuscript is
478 provided in Supplementary Table 1. cDNAs encoding N-terminally FLAG-tagged NINJ1
479 (full-length, delta 2-73, delta 142-152 and mutant D₁₄₇VAPR → A₁₄₇AAAA) were cloned into
480 pcDNA3.1 Zeo(+) (Thermo Fisher Scientific).

481

482 **Cell line authentication and quality control**

483 Cell lines were authenticated by short tandem repeat (STR) profiling and regular single
484 nucleotide polymorphism (SNP) fingerprinting. STR profiles are determined for each line using
485 the Promega PowerPlex 16 System. This is performed once and compared to external STR
486 profiles of cell lines (when available) to determine cell line ancestry. SNP profiles are performed
487 each time new stocks are expanded for cryopreservation. Cell line identity is verified by high-
488 throughput SNP profiling using Fluidigm multiplexed assays. SNPs were selected based on
489 minor allele frequency and presence on commercial genotyping platforms. SNP profiles are
490 compared to SNP calls from available internal and external data (when available) to determine or
491 confirm ancestry. All cells are tested for mycoplasma prior to and after cell cryopreservation
492 using two methods are used to avoid false positive/negative results: Lonza Mycoalert and
493 Stratagene Mycosensor. Cell growth rates and morphology are also monitored for any batch-to-
494 batch changes.

495

496 **BMDM stimulations**

497 Mouse bone marrow cells were differentiated into macrophages in Dulbecco's modified Eagle's
498 medium (DMEM) supplemented with 10% (v/v) low-endotoxin fetal bovine serum (FBS; Omega

499 Scientific) and 20% (v/v) L929-conditioned medium for 5 days. For stimulation, cells were
500 replated overnight at 1.0×10^5 cells/well in 96-well plates. For inflammasome stimulations, cells
501 were primed with Pam3CSK4 (1 $\mu\text{g}/\text{mL}$) for 5 h and then stimulated with 10 $\mu\text{g}/\text{mL}$ nigericin in
502 Opti-MEM I media (Thermo Fisher Scientific). For flagellin or LPS electroporation³⁹, 1.0×10^6
503 Pam3CSK4-primed BMDMs were electroporated with 1.0 μg LPS or 0.2 μg flagellin in 100 μL R
504 buffer using a neon 100 μL tip with 1,720 voltage, 10 width, 2 pulse settings. Electroporated cells
505 were added to 990 μL Opti-MEM I medium and cultured for 2 h. BMDMs treated with venetoclax
506 (25 μM for 6 h), doxorubicin (10 μM for 6 h), TNF plus ActD (20 ng/mL TNF, 500 ng/mL ActD
507 for 6 h), or TNF plus zVAD (100 ng/mL TNF, 20 μM zVAD for 16 h) were not primed. For lysis
508 controls, cells were lysed with 0.25% Triton-X100 in medium. Where indicated, BMDMs were
509 cultured with the indicated concentration of anti-NINJ1 clone 25¹ (mouse IgG2a; Genentech), anti-
510 NINJ1 clone D1 (mouse IgG2a; Genentech), anti-Ninjurin clone 50 (BD Biosciences BD610777,
511 raised against human NINJ1), or an isotype control mouse IgG2a (Thermo Fisher Scientific). Prior
512 to addition to cells, anti-Ninjurin clone 50 and isotype control mouse IgG2a antibodies were
513 dialyzed against PBS to remove sodium azide using Slide-A-Lyzer MINI Dialysis Device with a
514 10K MWCO (Thermo Fisher Scientific) according to manufacturer's instructions. Synthetic
515 peptides used were mouse NINJ1 aa 26-37 (PPRWGLRNRPIN, Genentech) and its sequence-
516 scrambled analogue (PWPPRRNRNGLI, Genentech). BMDMs were pretreated with antibody or
517 peptide for 10 min prior to addition of treatment.

518

519 **PMR and viability assays**

520 Culture medium was analyzed for LDH release with the CytoTox 96 Non-Radioactive
521 Cytotoxicity Assay (Promega). CellTiter-Glo reagent (ATP assay, Promega) was used for

522 detection of viable cells. Data for LDH and CellTiter-Glo assays was collected with an EnVision
523 2105 multimode plate using EnVision Manager 1.14.3049.1193 (PerkinElmer).

524

525 **Flow cytometry**

526 293T cells (ATCC, CRL-3216) cells were transfected with NINJ1 expression plasmids using
527 Lipofectamine 2000 (Thermo Fisher Scientific). Cells were stained with the following monoclonal
528 antibodies: anti-NINJ1 clone 25 mIgG2a (Genentech, 10 $\mu\text{g}/\text{mL}$), anti-NINJ1 clone D1 mIgG2a
529 (Genentech, 10 $\mu\text{g}/\text{mL}$), anti-Flag-M2 (Millipore Sigma, 1:100), anti-Ninjurin clone 50 (BD
530 Biosciences, 10 $\mu\text{g}/\text{mL}$). Primary staining was followed by APC-conjugated anti-mouse IgG
531 (Thermo Fisher Scientific, 1:300), and then propidium iodide (PI; 2.5 $\mu\text{g}/\text{mL}$; BD Biosciences).
532 Live PI⁻ cells were analyzed in a FACSymphony (Becton Dickinson). Data was acquired using
533 BD FACSDiva Software v9.1, and analyzed using FlowJo v10.8.1. Representative FACS gating
534 strategies and contour plots with outliers are shown in Supplementary Figs. 2, 3, and 4.

535

536 **DD-150 dye release assay**

537 BMDMs were loaded with fluorescein isothiocyanate-dextran (DD-150, MilliporeSigma) using a
538 100 μL Neon tip (Thermo Fisher Scientific). 5.0×10^6 BMDMs were electroporated in 120 μL R
539 buffer plus 12 μL 50 mg/mL DD-150. Prior to plating, BMDMs were washed with high-glucose
540 DMEM. Following stimulation, BMDMs were imaged in an IncuCyte S3 (Essen BioScience) at
541 10X magnification.

542

543 **Imaging of BMDM morphology**

544 BMDMs were plated on glass-bottom 96 MicroWell Optical Plates (Thermo Fisher Scientific).
545 Pam3CSK4-primed BMDMs were stimulated with 10 µg/mL nigericin in the presence or absence
546 of 10 µg/mL anti-NINJ1 antibody. Plates were imaged using a 60× Plan Fluor objective on an
547 ImageXpress Micro Confocal system running the MetaXpress v6.5.4.532 software and equipped
548 with an environmental controller and gas mixer to maintain cells at 37°C and 5% CO₂. Images of
549 the bright-field and transmitted light were imaged overnight every 15 min. Representative images
550 at the 8 h timepoint were processed using the using the scikit-image 0.19.2 python package.

551

552 **Immunofluorescence**

553 Clone D1 variable domains were cloned into the human Fab expression vector
554 1AP39.hIgG1.D.Fab (Genentech). Protein was expressed in *E. coli* and purified with a low
555 endotoxin level (<0.07 EU/mg). Pam3CSK4-primed BMDMs were cultured with 50 µg/mL D1
556 Fab and then stimulated with nigericin on glass-bottom 96 MicroWell Optical Plates (Thermo
557 Fisher Scientific). Cells were fixed with 4% paraformaldehyde in PBS and then permeabilized
558 with 0.1% Tween-20. Cells were blocked in PBS supplemented with 0.2% fish gelatin (Millipore
559 Sigma), 3% Bovine Serum Albumin and 0.1% Tween-20 for 1 h at room temperature, and then
560 labelled with anti-mouse NINJ1 clone 80 (rabbit IgG2b raised against the N-terminal extracellular
561 domain; Genentech, 2 µg/mL) at 4°C overnight. Bound antibody was revealed with an AF488-
562 conjugated anti-rabbit secondary (Thermo Fisher Scientific, 1:200) at room temperature for 1 h.
563 High resolution images were acquired with a Leica SP8X confocal laser scanning microscope
564 running Leica LAS X v3.5.7 software and equipped with a white light laser and a HC PL APO
565 CS2 oil immersion 40X lens of numerical aperture 1.3.

566

567 **Transient expression of NINJ1 in HEK293T cells**

568 cDNAs encoding untagged human or mouse NINJ1 were cloned into pcDNA3.1 Zeo(+).
569 HEK293T cells (2.6×10^4) were transfected with 50 ng plasmid plus 0.16 μ L Lipofectamine 2000
570 per well in 96-well plates in the presence of 20 or 200 μ g/mL of isotype control antibody, anti-
571 NINJ1 clone D1 (Genentech), or anti-NINJ1 clone D1 Fab (Genentech). YOYO-1 dye (Thermo
572 Fisher Scientific) was added at a final concentration of 200 nM at the time of transfection. IncuCyte
573 S3 images were scanned in the green channel every hour for at least 16 h and at $\times 10$ magnification.
574 Nuclear-ID Red DNA stain (Enzo Life Sciences) was added after the last time point and scanned
575 in the red channel. IncuCyte S3 2019A software was used to determine the total number of YOYO-
576 1⁺ cells and Nuclear-ID⁺ cells (total cells). % YOYO-1⁺ positive was calculated as the number of
577 YOYO-1⁺ cells divided by the total number of Nuclear-ID⁺ cells.

578

579 **Size exclusion chromatography (SEC)**

580 The C-terminally His6-tagged heavy chain Fab region (VH-CH1) and the untagged light chain of
581 anti-NINJ1 clone D1 and clone 25 were cloned into the mammalian expression vector pRK5J
582 (Genentech). Expi293F cells were transfected with pRK-FLAG-mNINJ1 alone, or co-transfected
583 with pRK-FLAG-mNINJ1, pRK5J-His6-VH-CH1 clone D1 (or pRK5J-His6-VH-CH1 clone 25),
584 and pRK5J-light chain clone D1 (or pRK5J-light chain clone 25) in a 2:1:2 plasmid ratio. NINJ1,
585 the NINJ1-clone D1 Fab complex, or the NINJ1-clone 25 Fab complex was purified with anti-
586 FLAG M2 resin (described above). For comparative SEC analysis, similar protein amounts and
587 volume of NINJ1, NINJ1-clone D1 Fab complex, or NINJ1-clone 25 Fab complex were injected

588 onto a Superose6 Increase 10/300 GL column (GE Healthcare). Data was collected with Unicorn
589 7.6 (Cytiva).

590

591 **Negative stain electron microscopy**

592 EM grids (400 mesh copper with continuous carbon, Electron Microscopy Sciences) were glow
593 discharged for 15 s at 10 mA using a GloQube glow discharge system (Quorum) before applying
594 4 μ L of sample diluted to approximately 0.1 mg/mL in SEC buffer (20 mM HEPES pH 7.5,
595 150 mM NaCl, 0.005% (w/v) LMNG, 0.0005% (w/v) CHS). After 1 min of incubation, the grid
596 was washed with distilled, deionized water, and stained with 1% uranyl acetate. After drying
597 completely, the grids were imaged in a Talos F200C equipped with a 4k \times 4k Ceta 16M Camera
598 (Thermo Fisher Scientific) using SerialEM Version 3.9.0. Images were recorded at a nominal
599 magnification of 45,000x (3.2 \AA per pixel).

600

601 **Liposomal cargo release assay**

602 Stocks of 1-palmitoyl-2-oleoyl-glycero-3-phosphocholine (POPC, Avanti Polar Lipids) and 1-
603 palmitoyl-2-oleoyl-sn-glycero-3-phospho-L-serine (sodium salt) (POPS, Avanti Polar Lipids)
604 were prepared in chloroform from dry powder. A lipid mixture of 80% POPC and 20% POPS was
605 generated, freeze dried, and hydrated with a solution of 10 mM Tris pH 8.0, 150 mM NaCl
606 containing the cargo, LANCE Eu-W1024 Biotin (PerkinElmer). The suspension was sonicated in
607 a water bath, freeze-thawed, and extruded using a Mini Extruder (Avanti Polar Lipids) fitted with
608 a Nucleopore 0.4 μ m membrane (Whatman) to yield large unilamellar vesicles. The liposomes
609 were purified by eluting through a column packed with Pierce Streptavidin Agarose resin (Thermo
610 Fisher Scientific). Liposomes were destabilized by addition of 0.0005% LMNG/0.00005% CHS

611 (Anatrace). Cargo release assay was set up by mixing destabilized liposomes (25 μM in lipid
612 concentration, diluted from 6.4 mM stock) with 8 μM NINJ1 purified according to the protocol
613 above or 0.4 μM Melittin peptide (Anaspec). Streptavidin-Alexa Fluor 647 (Thermo Fisher
614 Scientific) was added to each well at a final concentration of 1 μM . Liposomes mixed with
615 0.0005% LMNG in ddH₂O were used as a control. All samples were loaded into wells of a
616 ProxiPlate (PerkinElmer). TR-FRET readout was recorded on an EnVision 2105 multimode plate
617 reader (PerkinElmer) using EnVision Manager 1.14.3049.1193 (PerkinElmer). A pre-read of each
618 plate was taken immediately after loading the wells, and each plate was subsequently incubated
619 overnight at room temperature. After ~15 hours of incubation, another reading was taken, followed
620 by full digestion of the liposomes by addition of 1% Cholamidopropyl]dimethylammonio)-2-
621 hydroxy-1-propanesulfonate (CHAPSO, Anatrace) to each well. A final read was recorded
622 representing 100% cargo release. Results were converted to percentage cargo released per well
623 and background control subtracted.

624

625 **Stimulant-induced liver injury models**

626 In the TNF plus D-Gal model, liver injury was induced in females aged 8 to 14 weeks by ip
627 injection of 700 mg kg⁻¹ D-Gal (MilliporeSigma) and 30 μg kg⁻¹ mouse TNF (Genentech) unless
628 otherwise indicated. Serum was collected after 6-7 h. Where indicated, 8 to 14 weeks old age
629 matched C57BL/6J female (Jackson Labs) mice were dosed by ip injection with 50 mg kg⁻¹ body
630 weight of mouse anti-NINJ1 clone D1 antibody or isotype control anti-gp120 mouse IgG2a
631 monoclonal antibody (Genentech) at 2 h before TNF plus D-Gal. For ConA or anti-Fas mAb (Jo2)
632 treatment, liver injury was induced in males aged 9 to 11 weeks by intravenous injection with
633 either 20 mg kg⁻¹ body weight of Concanavalin A (Millipore Sigma) or 0.5 μg g⁻¹ body weight of

634 anti-Fas (anti-CD95 clone Jo2, BD Biosciences), respectively, unless otherwise indicated. Serum
635 was collected after 8 or 18 h for ConA, and after 5 h for anti-Fas. For antibody pre-treatment, 9 to
636 11 weeks old C57BL/6N male mice (Charles River Labs) were treated with the indicated mAbs as
637 described above. Serum ALT and AST were measured in a serum chemistry analyzer (Beckman
638 Coulter AU480). LDH in serum was measured with the CytoTox 96 Non-Radioactive Cytotoxicity
639 Assay. Enzyme-linked immunosorbent assays (ELISAs) were used to assay IL-18 (MBL
640 International) and HMGB1 (IBL). LDH assay and IL-18 and HMGB1 ELISA data was collected
641 with an EnVision 2105 multimode plate using EnVision Manager 1.14.3049.1193 (PerkinElmer).

642

643 **Histology**

644 Hematoxylin and eosin stained sections of *Rosa26^{Cre,ERT2/+}* livers were scored for hepatocellular
645 degeneration on a four-point scale based on the amount of viable tissue present as follows: (1)
646 multifocal hepatocellular injury with preservation of bridging portal tracts, (2) intermixed
647 populations of viable and degenerate cells throughout the liver, (3) bridging hepatocellular injury
648 with only the preservation of peri-portal hepatocytes, or (4) panlobular hepatocellular degeneration
649 with loss of lobular architecture. For scoring hepatocellular degeneration in antibody-treated mice,
650 six lobes were scored according to the following criteria: (0) no significant hepatocellular
651 degeneration, (1) multifocal cell death without loss of architecture, (2) non-bridging lobular
652 hepatocellular degeneration and loss of architecture, (3) bridging hepatocellular degeneration with
653 loss of architecture, or (4) diffuse hepatocellular degeneration. Scores from the 6 lobes were
654 averaged for a final score. To assess the persistence of swollen, degenerate hepatocytes, livers
655 were scored based on the predominant features of either cell loss with sinusoidal hemorrhage or
656 persistence of swollen degenerate hepatocytes. A three-tier scoring system was applied: (1)

657 predominant hepatocellular loss with sinusoidal hemorrhage, (2) mix of hepatocyte loss and
658 hemorrhage with regional aggregates of swollen, degenerate hepatocytes, or (3) predominant
659 preservation of swollen, degenerate hepatocytes. Scoring was performed in a random, blinded
660 manner.

661

662 **Immunohistochemistry**

663 Formalin-fixed, paraffin-embedded sections of liver were immunolabelled with rabbit anti-cleaved
664 caspase-3 antibody (Asp175, Cell Signaling Technologies, 0.05 µg/mL) or rabbit anti-NINJ1 clone
665 80 (5 µg/mL) using a discovery IHC platform (Roche). Conditions included CC1 standard antigen
666 retrieval (Roche), OmniMap detection (Roche) with diaminobenzidine, and hematoxylin
667 counterstain. Immunohistochemistry and histology images were acquired with Leica Application
668 Suit v4.6.0. Cleaved caspase-3 immunolabeling was scored according to the following matrix: (1)
669 multifocal individual or aggregates of labeled cells, (2) either extensive intermix of labeled and
670 unlabeled cells or centrilobular labeling with variable bridging, (3) extensive bridging cleaved
671 caspase 3 expression with only rims of unlabeled periportal hepatocytes, (4) diffuse hepatocellular
672 labeling. Scoring was performed in a random and blinded manner. NINJ1 immunolabeling was
673 qualitatively assessed in an unblinded manner.

674

675 **Ischemia-reperfusion liver injury**

676 Mixed-sex cohorts of 6 to 10 weeks old age C57BL/6J mice (Jackson Labs) were used in a 70 %
677 segmental ischemia-reperfusion model⁴⁰. Under isoflurane anesthesia, a sagittal midline
678 laparotomy was made, and a clamp placed on the portal vein and the hepatic artery to block blood
679 flow to the left and medial lobes of the liver. The clamp was removed after 1 h to allow for

680 reperfusion and the animal returned to their home cage. Following 6 hrs of reperfusion, the animal
681 was euthanized by cardiac puncture under general anesthesia and tissue collected for analysis.
682 Sham laparotomy where the vascular pedicle was exposed but not clamped was used as a negative
683 control. Where indicated, mice were dosed by ip injection with 50 mg kg⁻¹ antibodies 4 h before
684 induction of ischemia as described above. Animals were randomized to group and analyses
685 blinded. Serum LDH, ALT, AST levels were measured as described above. For histology, all
686 ischemic and reperfused liver lobes were collected, paraffin-embedded, sectioned at a thickness of
687 4 µm prior to staining with haematoxylin and eosin. Neutrophils were with rabbit anti-mouse Ly6G
688 (Cell Signaling Technology, 1:100) followed by biotinylated anti-rabbit secondary antibody
689 (Vector Laboratories, 1:200) and ABC (Vector Laboratories). DAB (Vector Laboratories) was
690 used to detect Ly6G staining. Tissue specimen processing and staining were conducted at the
691 Spatio-Temporal Targeting and Amplification of Radiation Response (STTARR) Innovation
692 Centre (Toronto, Canada). Slides were imaged using a 3DHistech Panoramic Flash II Slide
693 Scanner and visualized using either 3DHISTECH CaseViewer (RRID: SCR_017654) or HALO
694 Image Analysis Platform (RRID: SCR_018350; indica labs). To evaluate confluent necrosis within
695 the liver samples, the DenseNet classifier supervised machine learning algorithm (HALO Image
696 Analysis Platform) was trained to detect substantial areas of liver cell death using the haematoxylin
697 and eosin stain and applied to the entire sample. Neutrophils (Ly6G-positive) were counted using
698 QuPath (RRID: SCR_018257). Statistical testing was calculated using Prism 9.5.1 (GraphPad
699 Software Inc). Presented data are representative of at least three independent experiments. All
700 collected data was analyzed and a *P* value < 0.05 was considered statistically significant.

701

702 **Western blots**

703 Tissues were lysed in RIPA buffer (50 mM Tris pH 7.5, 150 mM NaCl, 2 mM EDTA, 1% NP-40,
704 0.5% SDS, 1× cOmplete Protease Inhibitor (Roche Applied Science) and PhosSTOP phosphatase
705 inhibitor (MilliporeSigma)) at 4 °C for 30 min. Tissues were mechanically disrupted with a bead
706 mill homogenizer (Omni International) and insoluble material was removed by centrifugation at
707 20,000 x g before addition of NuPAGE LDS sample buffer 4X (Thermo Fisher Scientific). Raw
708 images of uncropped gels are provided in Supplementary Fig. 1.

710 **GWAS**

711 Regional plots were generated using LocusZoom⁴¹ and GWAS data that used UK Biobank random
712 participant samples ($n = 363, 228$) and 35 blood and urine biomarkers^{14,32}
713 (<https://doi.org/10.1038/s41588-020-00757-z>).

715 **Statistics and figure preparation**

716 Unless otherwise specified, presented data are representative of at least two independent
717 experiments and means are of at least three biological replicates. Statistical analyses and number
718 of samples (n) are given in each figure panel. Mann–Whitney U -tests, t -tests and log-rank tests
719 were performed using GraphPad Prism 9.5.1 (GraphPad Software Inc).

720
721 No statistical methods were used to predetermine sample size. Sample sizes were chosen based
722 on prior experience and pilot experiments for detecting statistically significant differences
723 between conditions. For in vivo studies involving tamoxifen-treated animals, groups were
724 determined by genotype rather than treatment, and therefore not randomized. For TNF+D-Gal,
725 anti-Fas JO2, and ConA in vivo studies involving wt mice, animals were age- and sex- matched

726 and randomized to group. Experimental groups were assessed in the same experiment with
727 control groups to eliminate covariates. For animal procedures related to hepatic ischemia-
728 reperfusion injury mixed sex cohorts were used; animals were randomized to group and analyses
729 blinded.

730

731 **Data Availability**

732 The datasets generated during and/or analysed during the current study are available
733 from the corresponding authors upon reasonable request. Source data for animal studies are
734 provided with this paper. GWAS data was obtained from the UK Biobank study
735 (<https://doi.org/10.1038/s41588-020-00757-z>).

ACCELERATED ARTICLE PREVIEW

736 **References for methods**

- 737 33 Seibler, J. *et al.* Rapid generation of inducible mouse mutants. *Nucleic Acids Res* **31**, e12,
738 doi:10.1093/nar/gng012 (2003).
- 739 34 Chen, B. K., Rousso, I., Shim, S. & Kim, P. S. Efficient assembly of an HIV-1/MLV Gag-
740 chimeric virus in murine cells. *Proc Natl Acad Sci U S A* **98**, 15239-15244,
741 doi:10.1073/pnas.261563198 (2001).
- 742 35 Thery, C., Amigorena, S., Raposo, G. & Clayton, A. Isolation and characterization of
743 exosomes from cell culture supernatants and biological fluids. *Curr Protoc Cell Biol*
744 Chapter 3, Unit 3 22, doi:10.1002/0471143030.cb0322s30 (2006).
- 745 36 Lin, W. *et al.* Rapid identification of anti-idiotypic mAbs with high affinity and diverse
746 epitopes by rabbit single B-cell sorting-culture and cloning technology. *PLoS One* **15**,
747 e0244158, doi:10.1371/journal.pone.0244158 (2020).
- 748 37 Chen, Y. *et al.* Barcoded sequencing workflow for high throughput digitization of
749 hybridoma antibody variable domain sequences. *J Immunol Methods* **455**, 88-94,
750 doi:10.1016/j.jim.2018.01.004 (2018).
- 751 38 Shields, R. L. *et al.* High resolution mapping of the binding site on human IgG1 for Fc
752 gamma RI, Fc gamma RII, Fc gamma RIII, and FcRn and design of IgG1 variants with
753 improved binding to the Fc gamma R. *J Biol Chem* **276**, 6591-6604,
754 doi:10.1074/jbc.M009483200 (2001).
- 755 39 Kayagaki, N. *et al.* Noncanonical inflammasome activation by intracellular LPS
756 independent of TLR4. *Science* **341**, 1246-1249, doi:10.1126/science.1240248 (2013).
- 757 40 Abe, Y. *et al.* Mouse model of liver ischemia and reperfusion injury: method for studying
758 reactive oxygen and nitrogen metabolites in vivo. *Free Radic Biol Med* **46**, 1-7,
759 doi:10.1016/j.freeradbiomed.2008.09.029 (2009).
- 760 41 Pruim, R. J. *et al.* LocusZoom: regional visualization of genome-wide association scan
761 results. *Bioinformatics* **26**, 2336-2337, doi:10.1093/bioinformatics/btq419 (2010).

762
763 **Acknowledgements**

764 We thank Karen O'Rourke, Allison Bruce, Phoebe Chen, Shari Lau, Jian Jiang, Charles Jones,
765 Roderick Pata, Kathy Hotzel, Linda Rangell, Weibin Liang, Xiurong Zhang, Christine Tam, and

766 Wennie Chen for technical assistance, and Søren Warming, Alexis Rohou and Gözde Ulas for
767 helpful discussions. B.E.S. was funded by the Canadian Institutes for Health Research. Figures 1a
768 and Extended Data Fig. 3a, 7c were created with biorender.com.

769

770 **Author contributions**

771 N.K., I.B.S., O.S.K., and B.L.L. designed and performed experiments. K.A. and I.D. performed
772 protein purification, size exclusion chromatography and liposomal cargo release assay. M.C.J
773 performed negative stain electron microscopy. J.Z., J.L., E.S., and W.P.L. performed in vivo acute
774 hepatitis studies. S.W., Z.L., K.S., W.L., D.S., and R.L.K. generated antibodies. T.B. provided
775 GWAS analysis. I.B.S., O.S.K., and C.C. performed microscopy. J.D.W. analyzed tissue histology.
776 P.J. performed protein expression. J.M., S.Z., D.A., N.M.G., B.A.S., B.E.S., performed the hepatic
777 ischemia-reperfusion injury model. K.N. and V.M.D. contributed to experimental design and paper
778 editing. N.K. wrote the paper with input from all authors.

779

780 **Competing interests**

781 The following authors are employees of Genentech Inc.: Nobuhiko Kayagaki, Irma B. Stowe,
782 Kamela Alegre, Ishan Deshpande, Shuang Wu, Zhonghua Lin, Opher S. Kornfeld, Bettina L. Lee,
783 Juan Zhang, John Liu, Eric Suto, Wyne P. Lee, Kellen Schneider, WeiYu Lin, Dhaya Seshasayee,
784 Tushar Bhangale, Cecile Chalouni, Matthew C. Johnson, Prajakta Joshi, Kim Newton, Joshua D.
785 Webster, Ryan L. Kelly, Vishva M. Dixit

786

787 **Corresponding authors**

788 Correspondence and requests for materials should be addressed to kayagaki@gene.com or
789 dixit@gene.com.

790

791 **Extended Data Fig. 1 | Clone D1 inhibits PMR**

792 **a**, Graphs indicate LDH release in cultures of wild-type BMDMs after priming, and then
793 stimulation with nigericin for 16 h in the presence or absence (cont) of clone D1 Fab. Non-stim,
794 non-stimulated control. Bars indicate the mean. Circles indicate 3 biological replicates. Results
795 representative of 3 independent experiments.

796 **b**, Graphs indicate the percentage of YOYO-1⁺ HEK293T cells expressing NINJ1 when cultured
797 with or without (cont) clone D1 Fab. Circles are the mean \pm s.d. (shaded area) of 3 independent
798 replicates. Results are representative of 2 independent experiments.

799 **c**, Flow cytometry histograms of propidium iodide-negative HEK293T cells surface-stained with
800 anti-NINJ1 or anti-FLAG antibodies. Cells are mock transfected (light gray) or transfected with
801 human NINJ1 (dark gray). Results representative of 3 independent experiments.

802 **d**, Amino acid sequence alignment of human and mouse NINJ1. Predicted epitope of clone 25
803 (grey box) and clone D1 (blue box) are highlighted.

804 **e**, Graph shows the release of DD-150 from Pam3CSK4-primed BMDMs in **(a)** after nigericin
805 stimulation. Data are means (circles) \pm s.d. (shaded area). Circles indicate 3 biological replicates
806 ($n = 3$ animals). Results representative of 3 independent experiments.

807 **f**, Graphs indicate cell viability (top) and LDH release (bottom) in BMDM. Non-stim, non-
808 stimulated control. Bars indicate the mean. Circles indicate 3 biological replicates ($n = 3$ animals).
809 Results representative of 2 independent experiments.

810

811 **Extended Data Fig. 2 | Commercially available anti-NINJ1 antibody**

812 **a, c**, Graphs indicate LDH release in cultures of wild-type or *Ninjl*^{-/-} BMDMs after priming, and
813 then stimulation with nigericin for 4 h in the presence or absence (non) of 10 μ g/mL indicated

814 antibodies or 200 nM of peptides. Non-stim, non-stimulated control. Bars indicate the mean. BD
815 clone 50, BD Bioscience anti-Ninjurin clone 50. Circles indicate biological replicates ($n = 3$
816 animals); data were generated with bone marrow from 3 different mice. Results representative of
817 3 independent experiments.

818 **b**, Graph shows the release of DD-150 from Pam3CSK4-primed wild-type or *Ninj1*^{-/-} BMDMs
819 after nigericin stimulation in the presence or absence (non) of 10 $\mu\text{g}/\text{mL}$ indicated antibodies. Data
820 are means (circles) \pm s.d. (shaded area). Circles indicate biological replicates ($n = 3$ animals).
821 Results representative of 3 independent experiments.

822 **d**, Flow cytometry histograms of propidium iodide-negative HEK293T cells surface-stained with
823 indicated antibodies. Cells are mock transfected (light gray) or transfected with mouse NINJ1
824 (dark gray). Results representative of 3 independent experiments.

825

826 **Extended Data Fig. 3 | Biochemical analysis for NINJ1-anti-NINJ1 Fab complex**

827 **a**, Schematic of the procedures in Fig. 3c, d, e, and Extended Data Fig. 3b, c, d.

828 **b**, Coomassie blue staining of NINJ1 alone (retention volume 8.5-9 ml) and NINJ1-clone D1 Fab
829 complex (retention volume 15-15.5 ml) of Fig. 3c or NINJ1-clone 25 Fab complex of (**d**) (retention
830 volume 15.5-16 ml). Results representative of 2 independent experiments.

831 **c**, Negative stain electron microscopy of NINJ1-clone 25 Fab complex. Results representative of
832 2 independent experiments.

833 **d**, Size exclusion chromatography traces for purified NINJ1-clone 25 Fab complex. Results
834 representative of 3 independent experiments. Molecular weight standard marker positions are
835 pointed by arrows.

836

837 **Extended Data Fig. 4 | A link between *NINJI* and lower levels of serum AST and ALT in**
838 **Genome-wide Association Studies (GWAS)**

839 Regional plot of GWAS (UK Biobank random participants, $n = 363, 228$)^{14,32} showing correlation
840 of a *NINJI* single nucleotide polymorphism (rs7018885, purple diamond in chromosome 9 locus)
841 with lower serum AST (bottom) or ALT (top). *P* values were obtained from a two-sided test for
842 the null hypothesis that the effect of genotype (at each single nucleotide polymorphism) on the
843 ALT or AST values in a linear regression model was zero. *P* values are not adjusted for multiple
844 tests across the genome.

845

846 **Extended Data Fig. 5 | Characterization of tamoxifen-treated *Ninj1^{fl/fl}* *Rosa26-CreER^{T2}***
847 **mice.**

848 **a**, Immunoblots of mouse tissues at 2 weeks after tamoxifen dosing. Lanes represent different mice.
849 $n = 3$ mice per genotype.

850 **b**, Immunolabeling of *NINJI* (brown) in mouse liver sections. Scale bar, 25 μm . Results
851 representative of 3 mice of each genotype.

852

853 **Extended Data Fig. 6 | Clone D1 pretreatment limits hepatocellular degeneration and**
854 **caspase-3 cleavage in mice treated with TNF plus D-Gal**

855 **a**, Kaplan–Meier survival plots of mice injected with 25 $\mu\text{g kg}^{-1}$ TNF plus D-Gal. $n = 10$ mice per
856 group. *P* value two-tailed log-rank test. Results representative of 3 independent experiments.

857 **b**, Representative haematoxylin and eosin-stained liver sections of the mice in Fig. 4e. Scale bar,
858 50 μm . Arrows indicate swollen cells.

859 **c**, Histological scores of hepatocellular degeneration (left) and liver cell swelling (right) for the
860 mice in Fig. 4e. Untreated wild-type, $n = 5$ mice; wild-type dosed with antibody, TNF plus D-Gal,
861 $n = 10$ (left), $n = 9$ (right) mice. Lines represent the median, circles individual mice. P value two-
862 tailed Mann-Whitney U -test.

863 **d**, Liver sections from the mice in Fig. 4e after immunolabeling of cleaved caspase-3 (brown).
864 Graph indicates qualitative scoring of cleaved caspase-3 labeling. Untreated wild-type, $n = 5$ mice;
865 wild-type dosed with isotype control antibody, TNF plus D-Gal, $n = 10$ mice; Wild-type dosed
866 with clone D1 and TNF plus D-Gal, $n = 10$ mice. Lines represent the median, circles individual
867 mice. P value two-tailed Mann-Whitney U -test. Scale bar, 100 μm .

868

869 **Extended Data Fig. 7 | Clone D1 limits NINJ1-dependent PMR and inflammation in hepatitis**
870 **models.**

871 **a**, Mouse serum LDH, ALT, and AST. Where indicated, mice were dosed for 8 h with ConA.
872 Untreated wild-type, $n = 4$ mice; tamoxifen-treated $Ninj1^{+/+}$ $Rosa26\text{-CreER}^{\text{T2}}$, $n = 7$ mice;
873 tamoxifen-treated $Ninj1^{\text{fl/fl}}$ $Rosa26\text{-CreER}^{\text{T2}}$, $n = 9$ mice. a.u., arbitrary units. Lines represent the
874 mean, circles individual mice. P value two-tailed unpaired t -test, $P = 0.00000112$ (LDH), $P =$
875 0.0000427 (ALT), $P = 0.0000319$ (AST).

876 **b, e**, Wild-type mouse serum LDH, ALT, and AST. Where indicated, mice were dosed with 50
877 mg kg^{-1} antibody for 2 h before dosing with 15 mg kg^{-1} ConA for 18 h (**b**) or Jo2 anti-Fas for 5 h
878 (**e**). Untreated wild-type, $n = 5$ mice; wild-type dosed with isotype control antibody, $n = 8$ mice;
879 wild-type dosed with clone D1, $n = 7$ mice. Lines indicate the mean, circles individual mice. P
880 value two-tailed Mann-Whitney U -test (**b**) and two-tailed unpaired t -test (**e**).

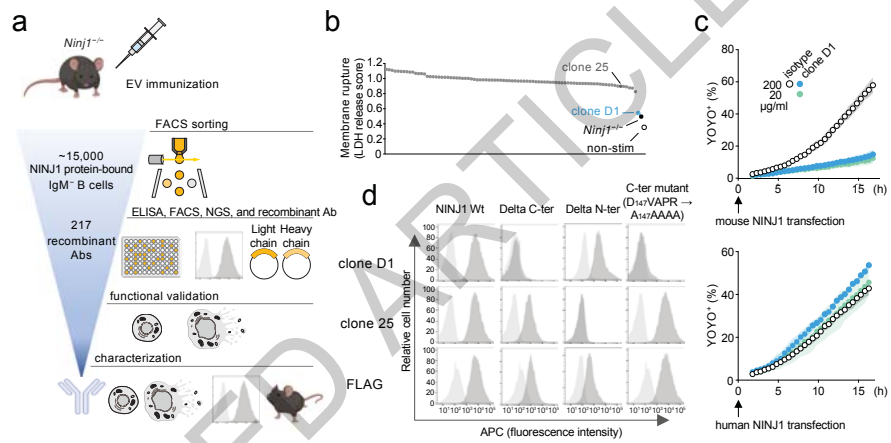
881 **c**, Schematic of the IRI procedure in (**d, h, i**).

882 **d**, Wild-type mouse serum LDH, ALT, and AST. Where indicated, mice were dosed with 50 mg
883 kg⁻¹ antibody for 4 h before IRI for 6 h. Untreated sham, *n* = 6 mice; wild-type dosed with isotype
884 control antibody, *n* = 9 mice; wild-type dosed with clone D1, *n* = 8 mice. Lines indicate the mean,
885 circles individual mice. *P* value two-tailed unpaired *t*-test.

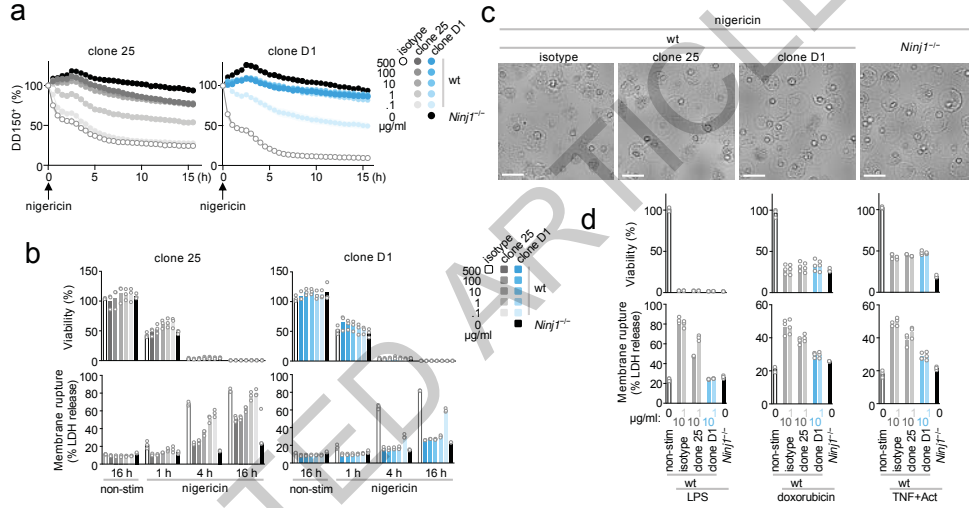
886 **f, g**, Liver sections with haematoxylin and eosin-staining (**f**) and immunolabeling of cleaved
887 caspase-3 (brown) (**g**) of mice dosed with 50 mg kg⁻¹ antibody for 2 h before dosing ConA for 6
888 h. Scale bar, 100 μm. Graphs indicate qualitative scoring of hepatocellular degeneration (**f**) and
889 cleaved caspase-3 labeling (**g**). Untreated sham, *n* = 4 mice; wild-type dosed with isotype control
890 antibody, *n* = 8 mice; wild-type dosed with clone D1, *n* = 8 mice. Lines indicate the median, circles
891 individual mice. *P* value two-tailed Mann-Whitney *U*-test.

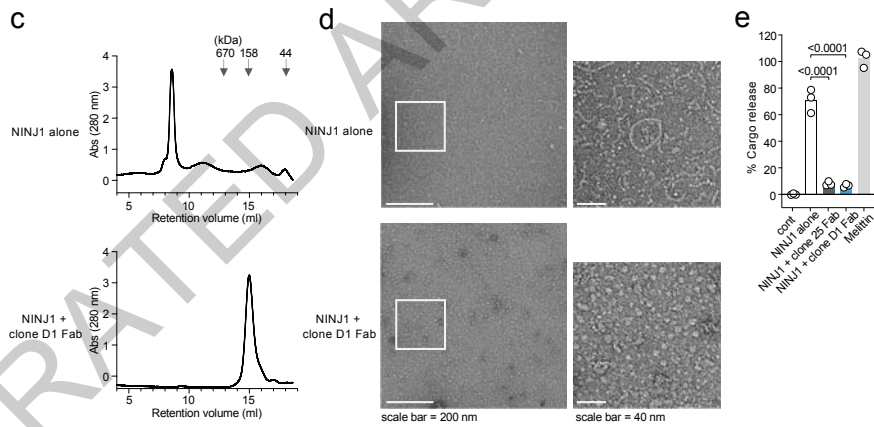
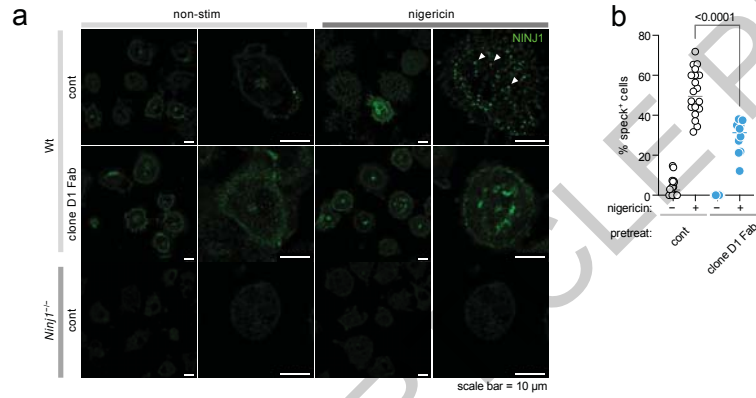
892 **h, i**, Liver sections with representative haematoxylin and eosin (**h**) and Ly6G (**i**) staining of the
893 mice in (**d**). Scale bar, 100 μm. Graphs indicate histological scoring of % confluent necrosis (**h**)
894 and Ly6G-positive cells (neutrophils) (**i**). Untreated sham, *n* = 6 mice; wild-type dosed with
895 isotype control antibody, *n* = 9 mice; wild-type dosed with clone D1, *n* = 8 mice. Lines indicate
896 the median, circles individual mice. *P* value two-tailed unpaired *t*-test.

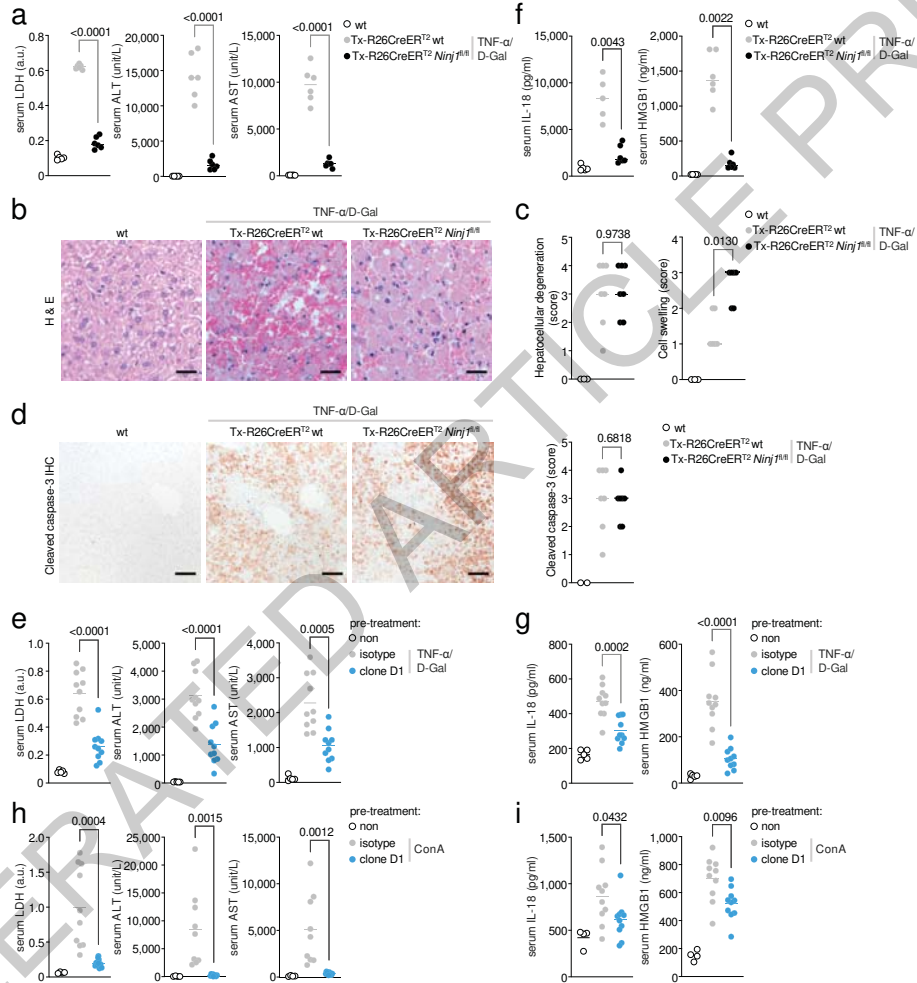
897

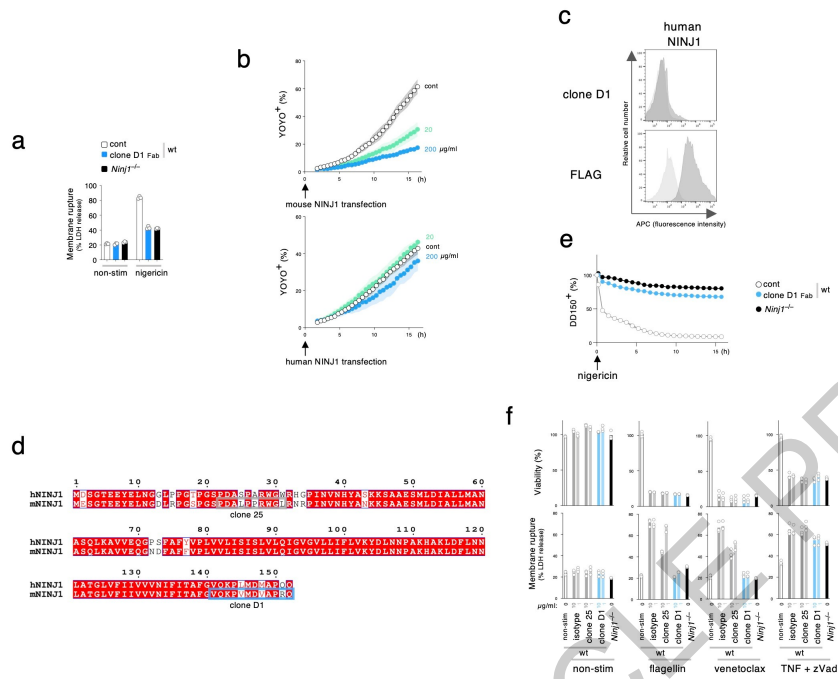


ACCELERATED ACCEPTED MANUSCRIPT PREVIEW

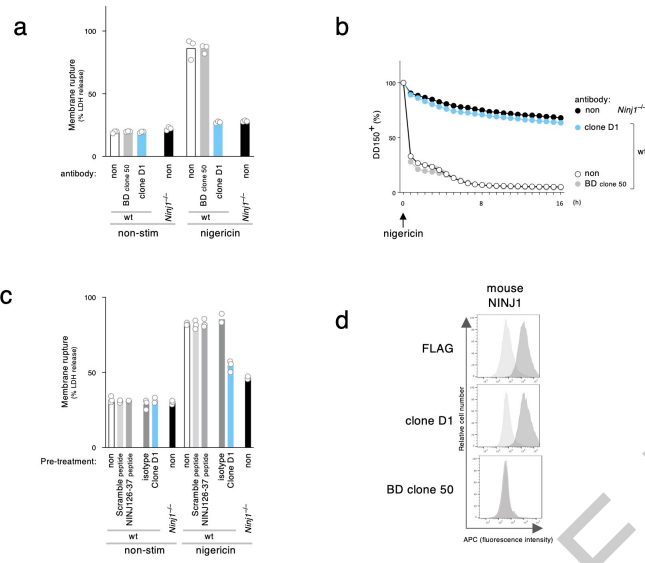






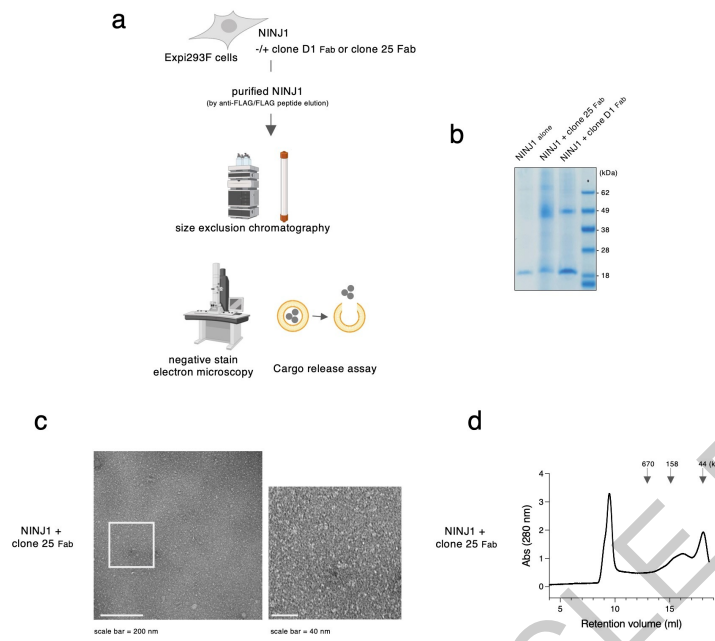


Extended Data Fig. 1

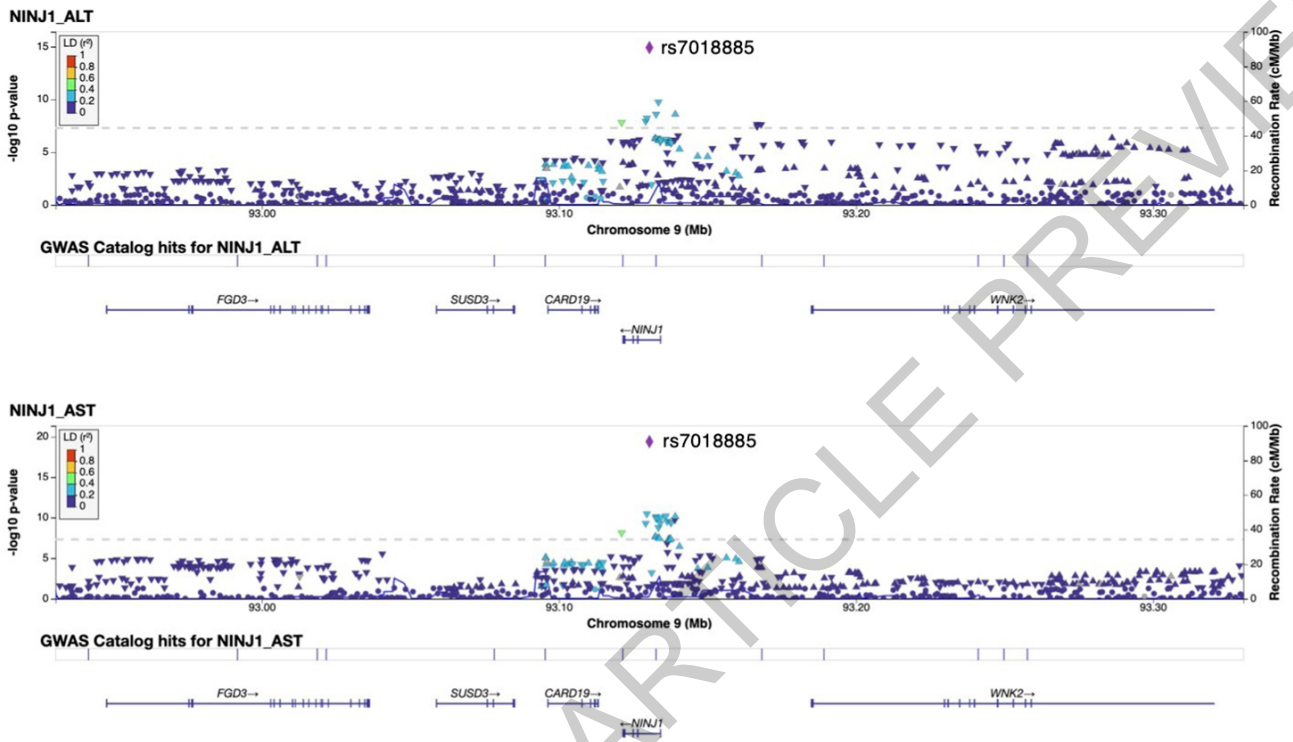


Extended Data Fig. 2

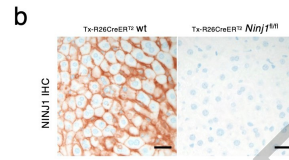
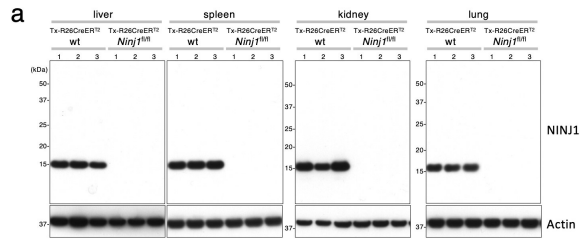
ACCELERATED ARTICLE PREVIEW



Extended Data Fig. 3

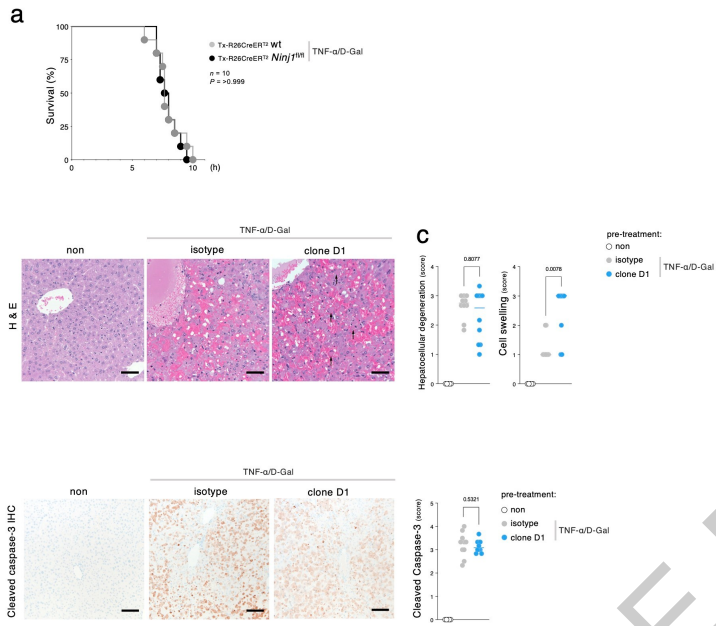


Extended Data Fig. 4



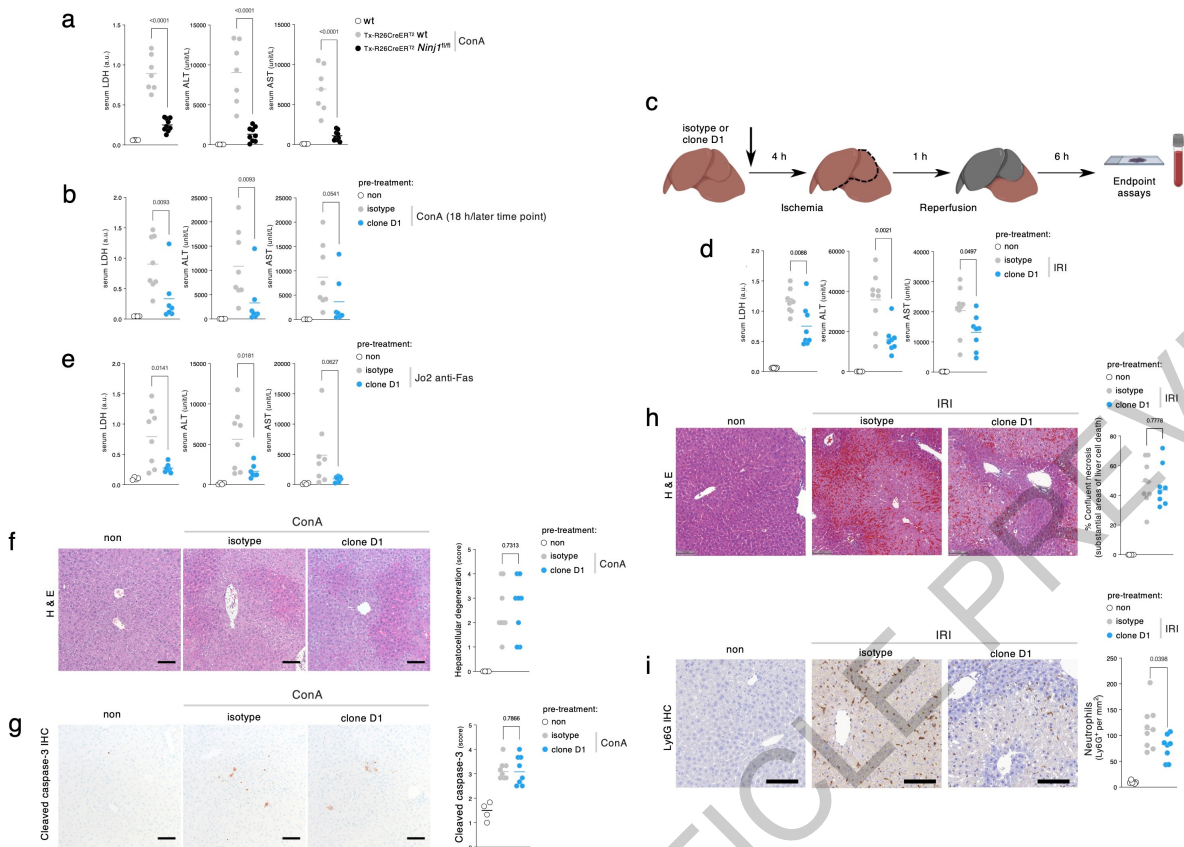
Extended Data Fig. 5

ACCELERATED ARTICLE PREVIEW



Extended Data Fig. 6

ACCELERATED ARTICLE PREVIEW



Extended Data Fig. 7

Reporting Summary

Nature Portfolio wishes to improve the reproducibility of the work that we publish. This form provides structure for consistency and transparency in reporting. For further information on Nature Portfolio policies, see our [Editorial Policies](#) and the [Editorial Policy Checklist](#).

Statistics

For all statistical analyses, confirm that the following items are present in the figure legend, table legend, main text, or Methods section.

n/a | Confirmed

- The exact sample size (n) for each experimental group/condition, given as a discrete number and unit of measurement
- A statement on whether measurements were taken from distinct samples or whether the same sample was measured repeatedly
- The statistical test(s) used AND whether they are one- or two-sided
Only common tests should be described solely by name; describe more complex techniques in the Methods section.
- A description of all covariates tested
- A description of any assumptions or corrections, such as tests of normality and adjustment for multiple comparisons
- A full description of the statistical parameters including central tendency (e.g. means) or other basic estimates (e.g. regression coefficient) AND variation (e.g. standard deviation) or associated estimates of uncertainty (e.g. confidence intervals)
- For null hypothesis testing, the test statistic (e.g. F , t , r) with confidence intervals, effect sizes, degrees of freedom and P value noted
Give P values as exact values whenever suitable.
- For Bayesian analysis, information on the choice of priors and Markov chain Monte Carlo settings
- For hierarchical and complex designs, identification of the appropriate level for tests and full reporting of outcomes
- Estimates of effect sizes (e.g. Cohen's d , Pearson's r), indicating how they were calculated

Our web collection on [statistics for biologists](#) contains articles on many of the points above.

Software and code

Policy information about [availability of computer code](#)

Data collection

Imaging (live and fixed) data captured using MetaXpress v6.5.4.532, Incucyte S3 2019A, or Leica LAS X v3.5.7. Immunohistochemistry and histology images were acquired with Leica Application Suite v4.6.0. Flow cytometry data were acquired with BD FACSDiva software v9.1 on a BD FACSymphony. Serum ALT and AST were measured in a serum chemistry analyzer (Beckman Coulter AU480). CellTiter-Glo, LDH, HMGB1 ELISA and IL-18 ELISA data were acquired with PerkinElmer EnVision Manager 1.14.3049.1193. Size exclusion chromatography data was collected with Unicorn 7.6 (Cytiva). Negative stain data collection was done using SerialEM Version 3.9.0. For hepatic IRI studies, slides were imaged using 3DHISTECH CaseViewer v2.4 (RRID: SCR_017654; indica labs, Albuquerque, US).

Data analysis

Plots were generated with Prism 9.5.1 (GraphPad Software Inc, La Jolla, CA; RRID:SCR_002798). Imaging data were analysed and prepared using scikit-image 0.19.2. Flow cytometry data were analysed with FlowJo version 10.8.1. Incucyte data was analysed with Incucyte S3 2019A. LocusZoom v0.12 was used to generate regional association plots. For hepatic IRI studies, slides were analysed with the HALO Image Analysis Platform 3.5.3577 (RRID: SCR_018350; indica labs, Albuquerque, US). To evaluate necrosis within the hepatic I/R liver samples, the DenseNet classifier supervised machine learning algorithm (HALO Image Analysis Platform 3.5.3577) was trained to recognize necrotic tissue using the haematoxylin and eosin stain and applied to the entire sample. To quantify immune cell infiltration, neutrophils (Ly6G-positive) were counted using QuPath v0.2.1 (RRID: SCR_018257).

For manuscripts utilizing custom algorithms or software that are central to the research but not yet described in published literature, software must be made available to editors and reviewers. We strongly encourage code deposition in a community repository (e.g. GitHub). See the Nature Portfolio [guidelines for submitting code & software](#) for further information.

Data

Policy information about [availability of data](#)

All manuscripts must include a [data availability statement](#). This statement should provide the following information, where applicable:

- Accession codes, unique identifiers, or web links for publicly available datasets
- A description of any restrictions on data availability
- For clinical datasets or third party data, please ensure that the statement adheres to our [policy](#)

The datasets generated during and/or analysed during the current study are available from the corresponding authors upon reasonable request. Source data for animal studies are provided with this paper. GWAS data was obtained from the UK Biobank study (<https://doi.org/10.1038/s41588-020-00757-z>).

Human research participants

Policy information about [studies involving human research participants and Sex and Gender in Research](#).

Reporting on sex and gender

Use the terms sex (biological attribute) and gender (shaped by social and cultural circumstances) carefully in order to avoid confusing both terms. Indicate if findings apply to only one sex or gender; describe whether sex and gender were considered in study design whether sex and/or gender was determined based on self-reporting or assigned and methods used. Provide in the source data disaggregated sex and gender data where this information has been collected, and consent has been obtained for sharing of individual-level data; provide overall numbers in this Reporting Summary. Please state if this information has not been collected. Report sex- and gender-based analyses where performed, justify reasons for lack of sex- and gender-based analysis.

Population characteristics

Describe the covariate-relevant population characteristics of the human research participants (e.g. age, genotypic information, past and current diagnosis and treatment categories). If you filled out the behavioural & social sciences study design questions and have nothing to add here, write "See above."

Recruitment

Describe how participants were recruited. Outline any potential self-selection bias or other biases that may be present and how these are likely to impact results.

Ethics oversight

Identify the organization(s) that approved the study protocol.

Note that full information on the approval of the study protocol must also be provided in the manuscript.

Field-specific reporting

Please select the one below that is the best fit for your research. If you are not sure, read the appropriate sections before making your selection.

- Life sciences Behavioural & social sciences Ecological, evolutionary & environmental sciences

For a reference copy of the document with all sections, see [nature.com/documents/nr-reporting-summary-flat.pdf](https://www.nature.com/documents/nr-reporting-summary-flat.pdf)

Life sciences study design

All studies must disclose on these points even when the disclosure is negative.

Sample size

Sample sizes are reported in the figure legends or the Methods section. No prior sample size calculation was performed for in vitro studies. For in vitro experiments involving BMDMs, bone marrow from at least 3 animals per genotype were analyzed for reproducibility. For in vitro experiments involving HEK 293T cells or liposome assays, three technical replicates were chosen per experiment. A minimum of three independent experiments was done for all experiments. This sample size was chosen to match previously published work by our group (Kayagaki et al, Nature 2015; Lee et al, J. Exp. Med. 2018, Kayagaki et al, Sci. Signal.) and is the norm in our field.

No prior sample size calculation was performed for in vivo studies. To account for greater variability in the in vivo studies, larger sample sizes (n=6-10) were used in the animal challenge studies (TNF+D-Gal, anti-Fas JO2, and ConA experiments) based on previous experience with the models used. These larger numbers were used to account for the greater variability between wild-type controls in these experiments. Sample sizes were chosen based on standards in the field and are sufficient based on the relatively large quantified differences between groups.

Data exclusions

For analysis of IL-18 in Fig 4f, serum from one animal was excluded in the tamoxifen-treated group due to insufficient serum quantity. For analysis of ALT & AST serum levels in Fig 4h, one sample was excluded from the isotype control treated group due to marked icterus.

Replication

All experiments were performed independently at least twice with similar results, as described in figure legends. All attempts at replication were successful. Independent experiments and biological replicates were used to ensure reproducibility of results.

Randomization

For in vivo studies involving tamoxifen-treated animals, groups were determined by genotype rather than treatment, and therefore not

Randomization	<p>randomized. For TNF+D-Gal, anti-Fas JO2, and ConA in vivo studies involving wt mice, animals were age- and sex- matched and randomized to group. Experimental groups were assessed in the same experiment with control groups to eliminate covariates.</p> <p>For animal procedures related to hepatic ischemia-reperfusion injury mixed sex cohorts were used; animals were randomized to group and analyses blinded.</p> <p>For all in vitro experiments, samples were not randomized because samples were not allocated into experimental groups.</p>
Blinding	<p>Imaging was performed blindly and automatically using an ImageXpress Micro Confocal or Incucyte system. Histological scoring and evaluation and serum analyses were performed blinded. For other experiments, mice and cell lines were picked and treated by the same individual, so blinding to genotype and treatment as well as during data collection and analysis was not possible.</p>

Reporting for specific materials, systems and methods

We require information from authors about some types of materials, experimental systems and methods used in many studies. Here, indicate whether each material, system or method listed is relevant to your study. If you are not sure if a list item applies to your research, read the appropriate section before selecting a response.

Materials & experimental systems

n/a	Involvement in the study
<input type="checkbox"/>	<input checked="" type="checkbox"/> Antibodies
<input type="checkbox"/>	<input checked="" type="checkbox"/> Eukaryotic cell lines
<input checked="" type="checkbox"/>	<input type="checkbox"/> Palaeontology and archaeology
<input type="checkbox"/>	<input checked="" type="checkbox"/> Animals and other organisms
<input checked="" type="checkbox"/>	<input type="checkbox"/> Clinical data
<input checked="" type="checkbox"/>	<input type="checkbox"/> Dual use research of concern

Methods

n/a	Involvement in the study
<input checked="" type="checkbox"/>	<input type="checkbox"/> ChIP-seq
<input type="checkbox"/>	<input checked="" type="checkbox"/> Flow cytometry
<input checked="" type="checkbox"/>	<input type="checkbox"/> MRI-based neuroimaging

Antibodies

Antibodies used	Supplementary Table 1 describes all antibodies used in this study.
Validation	<p>Any antibody validation of commercial primary antibodies is indicated in Supplementary Table 1 and can be found on the manufacturer's websites. Non-commercial antibodies generated for this study were validated as indicated below and within the manuscript.</p> <p>Clone D1-575 anti-NINJ1 antibody was validated for flow cytometry by comparing 293T cells transiently transfected with NINJ1 expression plasmids (this study, Fig1d)</p> <p>Clone 80 anti-NINJ1 antibody was validated for immunohistochemistry and immunofluorescence by comparing tissues or cells from WT and Ninj1 KO mice (this study)</p> <p>Clone 25 anti-NINJ1 antibody was previously validated for WB by comparing lysates from wild-type and NINJ1^{-/-} BMDMs (Kayagaki et al. 2021 Nature 591(7848):131-136)</p>

Eukaryotic cell lines

Policy information about [cell lines and Sex and Gender in Research](#)

Cell line source(s)	HEK293T cells (ATCC CRL-3216), Expi293F cells (Thermo Fisher Scientific, cat#A14527), BALB/3T3 clone A31 (ATCC CCL-163), CHO (Genentech), EL-4-B5 feeder cells (Roche)
Authentication	Cell lines were authenticated by short tandem repeat (STR) profiling and regular single nucleotide polymorphism (SNP) fingerprinting. STR profiles are determined for each line using the Promega PowerPlex 16 System. This is performed once and compared to external STR profiles of cell lines (when available) to determine cell line ancestry. SNP profiles are performed each time new stocks are expanded for cryopreservation. Cell line identity is verified by high-throughput SNP profiling using Fluidigm multiplexed assays. SNPs were selected based on minor allele frequency and presence on commercial genotyping platforms. SNP profiles are compared to SNP calls from available internal and external data (when available) to determine or confirm ancestry.
Mycoplasma contamination	Cells negative for mycoplasma.
Commonly misidentified lines (See ICLAC register)	Not used.

Animals and other research organisms

Policy information about [studies involving animals](#); [ARRIVE guidelines](#) recommended for reporting animal research, and [Sex and Gender in Research](#)

Laboratory animals	<p>Mice (<i>Mus musculus</i>) strains including Ninj1^{-/-} and WT littermates (Ninj1^{+/+}) (Kayagaki et al . 2021 Nature 591(7848):131-136), and Ninj1 fl/fl Rosa26.Cre.ERT2/+ and WT littermates (Ninj1 ^{+/+} Rosa26.Cre.ERT2/+) (this study) were maintained on a C57BL/6N genetic background.</p> <p>Ninj1 fl/fl Rosa26.Cre.ERT2/+ and WT littermates (Ninj1 ^{+/+} Rosa26.Cre.ERT2/+) were dosed with tamoxifen at 6 to 9 weeks of age.</p> <p>For TNF plus D-Gal studies 8 to 14 week old female mice were used. For TNF plus D-gal studies antibody treatment studies, 8 to 14 week old age matched C57BL/6J mice were used (Jackson Labs, strain #000664).</p> <p>For ConA and anti-Fas(JO2) studies, 9 to 11 week old male mice were used. For ConA and anti-Fas (JO2) studies involving antibody treatment, 9 to 11 week old age matched C57BL/6N male mice were used (Charles River Labs).</p> <p>For hepatic IRI studies, mixed-sex cohorts of 6 to 10 week old C57BL/6J wild-type animals were purchased from Jackson Laboratories (strain #000664).</p> <p>Mice were housed in individually ventilated cages within animal rooms maintained on a 14:10-hour, light:dark cycle with ad libitum access to food and water. Animal rooms were temperature and humidity-controlled, between 68-79°F and 30-70% respectively, with 10 to 15 room air exchanges per hour.</p>
Wild animals	The study did not involve wild animals.
Reporting on sex	TNF/Dgal in vivo studies were performed on 8 to 14 week old female mice. ConA and anti-Fas(JO2) studies were performed on 9 to 11 week old male mice. Hepatic IRI studies were performed on mixed-sex cohorts of 6 to 10 week old mice.
Field-collected samples	The study did not involve samples collected from the field.
Ethics oversight	<p>All animal procedures were conducted under protocols approved by the Genentech Institutional Animal Care and Use Committee in an Association for Assessment and Accreditation of Laboratory Animal Care (AAALAC)-accredited facility in accordance with the Guide for the Care and Use of Laboratory Animals and applicable laws and regulations.</p> <p>All animal procedures related to hepatic ischemia-reperfusion injury were conducted under protocols approved by the Animal Care Committee at The Hospital for Sick Children and in accordance with animal care regulation and policies of the Canadian Council on Animal Care.</p>

Note that full information on the approval of the study protocol must also be provided in the manuscript.

Flow Cytometry

Plots

Confirm that:

- The axis labels state the marker and fluorochrome used (e.g. CD4-FITC).
- The axis scales are clearly visible. Include numbers along axes only for bottom left plot of group (a 'group' is an analysis of identical markers).
- All plots are contour plots with outliers or pseudocolor plots.
- A numerical value for number of cells or percentage (with statistics) is provided.

Methodology

Sample preparation	HEK293T cells (ATCC) cells were transfected with NINJ1 expression plasmids using Lipofectamine 2000 (Thermo Fisher Scientific). Cells were stained with monoclonal antibodies, followed by APC-conjugated anti-mouse IgG (Thermo Fisher Scientific) and then propidium iodide (PI; 2.5 µg/mL; BD Biosciences). Live PI ⁻ cells were analyzed in a FACSsymphony (Becton 427 Dickinson).
Instrument	BD FACSsymphony
Software	Data was acquired using BD FACSDiva Software v9.1, and analyzed using FlowJo 10.8.1
Cell population abundance	No sorting was performed.
Gating strategy	Dead cells that stained with PI (BD Biosciences) were excluded from analyses of cells.

- Tick this box to confirm that a figure exemplifying the gating strategy is provided in the Supplementary Information.